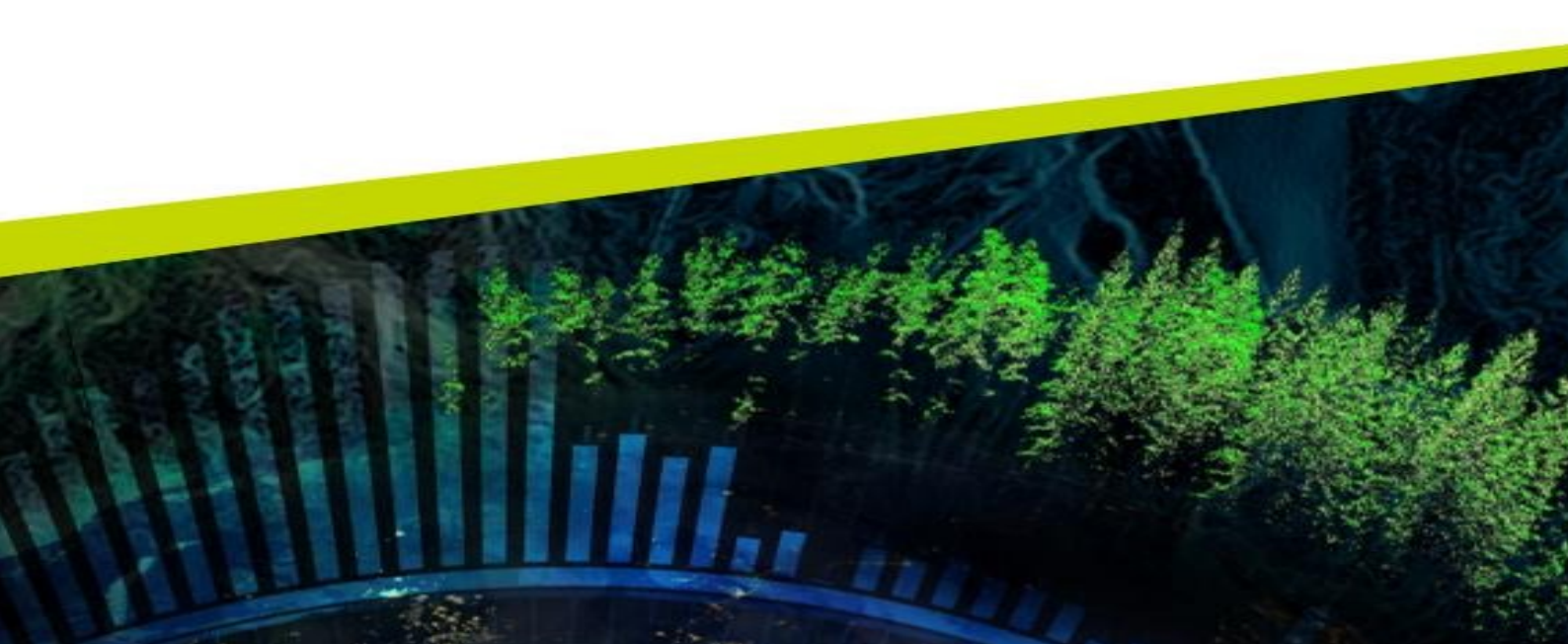




# Influence of Organic Acids on the Sorption of Phosphorus to Ferrihydrite and Imogolite-type Nanoparticles

Lisa Marie Deiglmayr

Master thesis project · 30 hp Swedish University of Agricultural Sciences, SLU Department of Soil and Environment Number in series: 2025:19 Uppsala, 2025



# Influence of Organic Acids on the Sorption of Phosphorus to Ferrihydrite and Imogolite-type Nanoparticles

Lisa Marie Deiglmayr

Supervisor Tove Florén, Swedish University of Agricultural Sci-

ences, Department of Soil and Environment

Supervisor

Jon-Petter Gustafsson, Swedish University of Agricul-

tural Sciences, Department of Soil and Environment

Assistant Supervisor Eva Oburger, University of Natural Resources and Life

Sciences, Vienna, Institute of Soil Research

Examiner Marie Spohn, Swedish University of Agricultural Sci-

ences, Department of Soil and Environment

**Credits** 30 credits

Level Second cycle, A2E

Course title Master thesis in Environmental Science

Course code EX0897

Programme/education Environmental Science - Soil, Water and

**Biodiversity** 

Course coordination dept Department of Soil and Environment

Place of publication Uppsala, Sweden

Year of publication 2025

Partnumber 2025:19

Series title Examensarbeten / Institutionen för mark och miljö,

SLU

Online publication https://stud.epsilon.slu.se

**Keywords** Proto-Imogolite, Ferrihydrite, Oxalate, D-Gluconate,

Adsorption, CD-MUSIC

#### **Swedish University of Agricultural Sciences**

Faculty of Natural Resources and Agricultural Sciences Department of Soil and Environment

# **Acknowledgement**

Above all, I would like to thank my supervisors, Tove Florén and Jon-Petter Gustafsson. Tove guided me so well through the experimental part of the work, especially the Proto-Imogolite synthesis, while Jon-Petter repeatedly helped me to understand VisualMINTEQ modelling. I wish to thank them both for their valuable input, encouragement and constant support. Thanks also to my co-supervisor Eva Oburger, whose questions encouraged me to critically re-examine my approach and motives. I want to thank my examiner Marie Spohn and my student-opponent Clara Kieschnick-Llamas for their great feedback and a special thanks goes to Ylva Bellander for the help in the lab and with the DOC measurements.

#### **Abstract**

Phosphorus (P) is an essential macronutrient for plant growth, yet its availability in forest soils can be limited by the strong adsorption onto mineral surfaces. This thesis studied the sorption behaviour of P to synthetic ferrihydrite (Fh) and proto-imogolite (PIM), two abundant secondary minerals in the B horizons of Swedish Podzols, as a function of pH. P sorption decreased with increasing pH for both Fh and PIM, due to a less positively charged surface. P sorbed more strongly to PIM at pH >5.5 than to Fh, but less below pH 4.9, due to dissolution of PIM. Furthermore, the influence of two organic acid anions, D-gluconate (GL) and oxalate (Ox) was tested. Both acid anions were found to be able to mobilise P from Fh and PIM and thus make it more bioavailable to plants. Ox was more efficient at mobilising P than GL, especially from PIM. Its main mechanism was through the dissolution of the mineral, with a higher ability to dissolve PIM than Fh, thus releasing more P. GL could not dissolve the minerals when P was present. It hindered P sorption through competition for the same binding sites. Experimental data from single sorbent system were used to optimise complexation constants for the Fh CD-MUSIC Model (Gustafsson and Antelo 2022) and the PIM Basic Stern Model (Florén et al. in preparation). While modelled sorption behaviour to Fh was tolerable, sorption to PIM could not be accurately portrayed due to experimental errors as well as potentially inaccurate fundamental properties used as input. Only the P sorption to PIM in the single sorbent system could be successfully represented.

# **Popular Science Summary**

This thesis studied the behaviour of phosphorus (P) in soil. For plant growth, not only water and light are required, but also nutrients. Phosphorus is such an essential nutrient that is part of their DNA or energy transfer molecules, that play a part in photosynthesis. Understanding the bioavailability of P is crucial for sustainable forest management in order to avoid P deficiency or overfertilisation by providing precise fertilizer recommendations. P can only be taken up by the plant in its dissolved form of negatively charged ions (e.g. phosphate PO<sub>4</sub><sup>3-</sup>). Most P in soils is originally bound in minerals. When they dissolve, phosphate ions are set free. In soils, iron minerals, such as ferrihydrite (Fh) and aluminium minerals, like proto-Imogolite (PIM) are present. In Swedish forest soils, they are especially abundant. Both of them can have a charged surface depending on the pH. Towards more acidic pH values, they take up protons (H<sup>+</sup> ions), resulting in positive charges that then attract the negatively charged phosphate ions. The ions can now be adsorbed to those surfaces and are thus stuck to the solid phase of the soil and are not available to the plants anymore. Nevertheless, this adsorption process is reversible. Plants have evolved mechanisms to detach the phosphate ions again, so they can take them up. One of these is the release of small organic acids that have the ability to dissolve the minerals, thus setting P free or compete with the phosphate ions for the same binding sites. In the soil solution those acids are present as their respective negatively charged anion. So, they can bind to the mineral's surface in the same manner as the phosphate ions. The site is then occupied and the phosphate thus stays in solution available for plant uptake. In this thesis, Fh and PIM were synthesised. They were exposed to a fixed amount of phosphate solution for 19 hours at different pH values between 3 and 8. The suspensions were filtered and the remaining P concentration was measured to backcalculate the amount that was adsorbed to the mineral. The same was repeated with the two organic acid anions oxalate (Ox) and D-gluconate (GL). Furthermore, the competing systems of phosphate and one acid anion was tested to assess their ability to release P into solution.

P sorption decreased with an increasing pH due to less positively charged surfaces. Furthermore, the P sorption was stronger to PIM than to Fh above pH 5.5 due to a higher surface area of PIM, resulting in more sorption sites. Below pH 4.9, P sorption dropped for PIM, because the mineral started dissolving at lower pH values. Both acid anions were able to reduce the P sorption to both minerals, releasing it into solution, making it more available to plants. The effect was bigger for PIM, owing to its weaker stability compared to Fh. Ox could release more P than GL, especially from PIM. GL released P only through competition, while Ox could also dissolve the minerals, particularly at lower pH. GL was not able to dissolve them in competing systems with P.

Those results were tried to be replicated with a model in order to test the model's ability to predict the P behaviour in soil, so it makes it easier to assess a site in terms of fertility without having to take soil samples and analyse them. While the model for Fh gave tolerable results, the model for PIM could not accurately reproduce experimental data. This was due to experimental issues used as input data and the model used which is still under development and whose basic properties may therefore need to be revised.

# **Contents**

Lis	st of 7	Tables	ix
Lis	st of F	Figures	x
Αk	brevi	iations	хi
1	Intro	oduction	1
2	Aim	and Limitations	3
3	3.1 3.2	kground Iron and Aluminium (hydr)oxides	<b>5</b> 5 7 8
	3.3 3.4	P-Solubilising Mechanisms	10 12
4	4.1 4.2 4.3	Equipment	15 16 16 16 16 17 17
	4.4	Modelling with Visual MINTEQ	18
5	<b>Res</b> i 5.1	Experimental Results  5.1.1 P Sorption in the Single Sorbent Systems  5.1.2 Difference in Acid Sorption  5.1.3 Sorption in the Competitive Systems  5.1.4 Storage Time of Fh  5.1.5 Contamination through Filters  Modelling Results	20 20 20 21 24 27 29 30
		5.2.1 Modelling Ferrihydrite	30 31
6	Con	clusion	33
Bi	bliog	raphy	35
Αr	pend	lix	ı

# **List of Tables**

1	Structures and protonation constants for oxane and $D$ -glucome acid	12
2	Sites in the Fh CD-MUSIC Model (Gustafsson and Antelo 2022). A small $c$ denotes corner-sharing complexes, a small $e$ edge-sharing complexes, and a small h in brackets high-affinity sites	18 19
3	Best-fit results for surface complexation reactions	19
4	Series: Ferrihydrite + Phosphorus (Day 19). Amount of stock solutions added in pH dependent batch experiments with measured pH, DOC and Fe and P content from ICP-OES. Empty cells indicate that no addition of the respective component was made or that no measurement was taken for the results. DOC or P cells with a value of 0 indicate that no OC or P was added in this series, although this was not explicitly measured to confirm this	VI
5	Series: Ferrihydrite + Phosphorus (Day 0). Amount of stock solutions added in pH dependent batch experiments with measured pH, DOC and Fe and P content from ICP-OES. Empty cells indicate that no addition of the respective component was made or that no measurement was taken for the results. DOC or P cells with a value of 0 indicate that no OC or P was added in this series, although this was not explicitly measured to confirm this	VII
6	Series: Ferrihydrite + <i>D</i> -Gluconate. Amount of stock solutions added in pH dependent batch experiments with measured pH, DOC and Fe and P content from ICP-OES. Empty cells indicate that no addition of the respective component was made or that no measurement was taken for the results. DOC or P cells with a value of 0 indicate that no OC or P was added in this series, although this was	VII
7	not explicitly measured to confirm this	VIII
8	although this was not explicitly measured to confirm this	IX
9	measured to confirm this	X
	not explicitly measured to confirm this	XI

10	Series: Proto-Imogolite + Phosphorus. Amount of stock solutions added in pH	
	dependent batch experiments with measured pH, DOC and Al, Si and P content	
	from ICP-OES. Empty cells indicate that no addition of the respective component	
	was made or that no measurement was taken for the results. DOC or P cells with	
	a value of 0 indicate that no OC or P was added in this series, although this was	
	not explicitly measured to confirm this	XII
11	Series: Proto-Imogolite + D-Gluconate. Amount of stock solutions added in	
	pH dependent batch experiments with measured pH, DOC and Al, Si and P	
	content from ICP-OES. Empty cells indicate that no addition of the respective	
	component was made or that no measurement was taken for the results. DOC	
	or P cells with a value of 0 indicate that no OC or P was added in this series,	
	although this was not explicitly measured to confirm this	XIII
12	Series: Proto-Imogolite + Phosphorus + <i>D</i> -Gluconate. Amount of stock solutions	
	added in pH dependent batch experiments with measured pH, DOC and Al,	
	Si and P content from ICP-OES. Empty cells indicate that no addition of the	
	respective component was made or that no measurement was taken for the results.	
	DOC or P cells with a value of 0 indicate that no OC or P was added in this	
	series, although this was not explicitly measured to confirm this	XIV
13	Series: Proto-Imogolite + Oxalate. Amount of stock solutions added in pH	
	dependent batch experiments with measured pH, DOC and Al, Si and P content	
	from ICP-OES. Empty cells indicate that no addition of the respective component	
	was made or that no measurement was taken for the results. DOC or P cells with	
	a value of 0 indicate that no OC or P was added in this series, although this was	
	not explicitly measured to confirm this	XV
14	Series: Proto-Imogolite + Phosphorus + Oxalate. Amount of stock solutions	
	added in pH dependent batch experiments with measured pH, DOC and Al,	
	Si and P content from ICP-OES. Empty cells indicate that no addition of the	
	respective component was made or that no measurement was taken for the results.	
	DOC or P cells with a value of 0 indicate that no OC or P was added in this	
	series, although this was not explicitly measured to confirm this	XVI

# **List of Figures**

2	(8 nm diameter). The close-up displays no surface depletion (no SD) of Fe2 and Fe3 sites, while b) shows it with surface depletion (SD) (Boily and Song 2020). Schematic representation of the structure of an imogolite nanotube with A)	6
	Al-rich and (B) Si-rich local structure. Si sites are indicated by Qn, n (0-4) is the number of directly linked Si tetrahedrons (Levard and Basile-Doelsch 2016)	7
3	Biogeochemical processes of P (Tuyishime 2022)	9
4 5	Important fluxes and pools of LMWOAs (Jones 1998)	11
6	Graphical abstract of the experimental work	16
	•	10
7	a) Phosphorus sorption and b) dissolved Fe and Al as a function of pH in the single sorbent systems. Empty black circles represent data for the series Fh+P, empty red diamonds for the series PIM+P	20
8	Dissolved Al:Si ratio as a function of pH in the system PIM+P	21
9	Acid anion sorption to a) Fh and b) PIM as a function of pH in the single sorbent systems; c) dissolved Fe and d) dissolved Al in the single sorbent systems. For data of the competitive systems see Figure 10 and Figure 11. Systems with Fh are presented as circles, systems with PIM as diamonds. GL-2 and Ox-2 refer to	
10	data points of only the second replicate (see section 5.1.5) Sorption/Dissolution behaviour as a function of pH for Fh (left, circle) and PIM (right, diamond): Amount of a) P sorbed to Fh, b) P sorbed to PIM, c) dissolved Fe, d) dissolved Al, e) dissolved Si. Full symbols represent a competitive system, while empty symbols represent the individual systems. Lines are the modelling	22
11	results from Visual MINTEQ	25 26
12	Difference in storage time for Fh: a) Fh+P, b) Fh+Ox, c) Fh+P+GL, d) Fh+GL and Fh+P+GL. The longer storage time is shown in grey in each case. Full circles represent a competitive system, while empty circles represent the individual	28
13	oC contamination through the 10 kDa centrifugal devices in the series of a) PIM+GL, b) PIM+P+GL, c) PIM+Ox, d) PIM+P+Ox. The replicate that was not used for further analysis is displayed in grey. Full diamonds represent a	
	competitive system, while empty diamonds represent the individual systems	29

#### **Abbreviations**

Al Aluminium

**BS** Basic Stern

Ca Calcium

**C** Carbon

**CD-MUSIC** Charge Distribution - Multisite Complexation

**DOC** Dissolved Organic Carbon

**EMF** Ectomycorrhizal Fungi

**Fh** Ferrihydrite

FTIR Fourier Transform Infrared Spectroscopy

**GL** *D*-Gluconate

ITN Imogolite-Type Nanoparticles

IC Inorganic Carbon

ICP-OES Inductively Coupled Plasma Optical Emission Spectroscopy

**Fe** Iron

**LMWOA** Low Molecular Weight Organic Acid

N Nitrogen

OC Organic Carbon

Ox Oxalate

**O** Oxygen

**P** Phosphorus

**PZC** Point of Zero Charge

PIM Proto-Imogolite

Si Silicon

**SSA** Specific Surface Area

Total Carbon

**TOC** Total Organic Carbon

**XRD** X-Ray Diffraction

# 1 Introduction

Phosphorus (P) is an essential macronutrient to sustain life on Earth and its availability plays an important role in sustainable forest management. P is often added to soils to improve their fertility. Understanding the mechanisms of the behaviour of P is crucial to predict its availability for the uptake in plants and organisms, also under changing environmental conditions.

A lot of temperate and boreal forest soils in northern Europe developed after the last glacial period 8000 – 15 000 years ago (Andersson et al. 2014). They are therefore considered to be rather young soils, still containing a lot of apatite and are thus mainly not limited by P but by nitrogen (N). Nevertheless, while N can be fixed by microorganisms from the atmosphere, there is little intake of P in soils. In recent decades, atmospheric N deposition has increased, enriching some forest ecosystems with N, potentially increasing the risk of N leaching, which in turn could lead to P becoming the limiting nutrient (Akselsson et al. 2008; Binkley and Högberg 2016). Furthermore, the harvesting of biomass, especially of whole-trees, but also of the stems, could lead to P losses and thus P becoming the critical nutrient. On 14 550 Swedish sites in southern Sweden, it was shown that more than 1 kgh<sup>-1</sup> is lost annually from forestry (Akselsson et al. 2008). It is therefore of interest to know the bioavailability of P to predict forest growth and to guarantee sustainable forest management.

In the B horizon of Swedish forest soils, mostly in Podzols, dissolved P species are mainly adsorbed to iron (Fe) and aluminium (Al) (hydr)oxides, such as ferrihydrite (Fh) and imogolite-type nanoparticles (ITN). The term ITN includes allophane, imogolite and their common precursor proto-imogolite (PIM). ITN and Fh both have a large specific surface area (SSA), similar surface-charge properties and possess singly coordinated surface groups that can form strong surface complexes with oxyanions. Nevertheless, while Fh and its P sorption has been frequently studied (Gustafsson and Antelo 2022; Mallet et al. 2013; Wang et al. 2015; Tiberg 2016; Jones and Brassington 1998), ITNs that potentially play a big role in determining P availability are only starting to be investigated. P has been found to bind more strongly to allophane than to Fh (Parfitt 1989) and ITNs, which are dominated by PIM, have been identified as main sorbent surface for P anions in Swedish Podzols (Tuyishime et al. 2022; Tuyishime et al. 2024; Florén et al. 2025).

Additionally, plants have developed mechanisms to acquire P, for example through changes in their root architecture, or the release of organic acids by microorganisms, such as mycorrhizal fungi (Doydora et al. 2020; Schreider et al. 2022). While Klotzbücher et al. (2020) detected that beech could not take up P from goethite mineral surfaces, ryegrass was shown to be able to acquire adsorbed P from goethite and gibbsite (Amadou et al. 2022).

In order to understand and predict sorption behaviour, particularly in relation to nutrient availability and the movement of contaminants, reliable models are essential. Geochemical modelling allows to quantitatively evaluate complex processes and can help to figure out the outcome of geochemical reactions over a long time scale, far longer than the possible range in the laboratory (Zhu and Anderson 2002). Within the Visual MINTEQ Programme (Gustafsson 2024b), an adsorption model for Fh has been developed by Hiemstra and Zhao (2016) and further optimised by Gustafsson and Antelo (2022). Because there is no similar model for ITNs yet, its sorption behaviour is often assumed to resemble that of Fh or gibbsite, which may not accurately reflect experimental results (Florén et al. 2025).

Therefore, in order to better predict and understand the mechanisms behind the availability of P, this thesis will investigate the sorption of P to synthesized Fh and PIM surfaces and focuses on how organic acids influence that behaviour. Based on the findings of Parfitt (1989), Tuyishime et al. (2024), and Florén et al. (2025) it is hypothesised that P will be sorbed more strongly to PIM than to Fh. Since ITN are less thermodynamically stable than Fh, organic acids are thought to dissolve PIM more easily and thus liberate a higher amount of sorbed P. The results will then be implemented in a Visual MINTEQ model to further optimise it and predict P availability in the future.

# 2 Aim and Limitations

The overall aim of this thesis was to improve the understanding of P sorption to Fe- and Al-(hydr)oxides to improve fertilizer recommendations and prevent eutrophication.

The specific objectives were to:

- Investigate P sorption to the very common secondary minerals in the B horizons of Podzols, Fh and ITNs. While Fh is already more studied, little is known about ITNs, which were previously shown to play a major role in the adsorption of P. PIM is chosen as the main adsorbent surface within ITNs.
- Analyse the effect of organic acids (namely *D*-gluconic and oxalic acid) on the sorption of P to Fh and PIM, since those are released by soil organisms in order to make P available for uptake.
- Use the results from batch experiments in Visual MINTEQ to evaluate the model's ability to predict P solubility and optimise constants to better predict the behaviour of P in soils.

#### Limitations

Generally, as no experiments were carried out with real soil samples, the results of the project may have certain limitations in terms of accuracy. In a natural system, where other minerals and organic matter are also present, interactions are very complex.

Factors not accounted for in this thesis:

- Interaction between mineral surfaces or organic matter are not taken into account, as well as other ions naturally occurring in the environment that can lead to impurities in the mineral which in turn might affect its particle size, solubility, surface structure and thus its ability to sorb anions (Cismasu et al. 2011).
- Since Fe- and Al-(hydr)oxides can interact with each other through coprecipitation, sequential precipitation and agglomeration, phases comprising both minerals can possess different properties (Tiberg 2016).
- Only simple organic acids were used. Although these are less complex than humic and fulvic acids, their sorption properties can be quite similar and they have been shown to play an important role in nutrient acquisition (Evanko and Dzombak 1999).
- Competition with other ions.
- Batch experiments were carried out at 8 °C to prevent degradation of the organic acids by microbes. In reality, soil temperature varies with depth, season and latitude. At a soil depth between 10 cm to 20 cm soil temperature at four sites in Sweden ranged from 0-2 °C in winter to 8-12 °C in summer. However, with rising temperatures in air due to climate change, soil temperature is also expected to increase (Jungqvist et al. 2014). The alternative of using azide was considered. However, since it is highly reactive, rather high concentrations of the acid anion would likely be needed to see a noticeable response. This would affect the whole sorption process and consequently the amount of adsorption.

Furthermore, azide anions will probably form outer-sphere complexes that need to be accounted, so extra time would have been needed to quantify this effect in order to build a credible model. Due to the limited time frame of the thesis, this option was therefore ruled out.

# 3 Background

# 3.1 Iron and Aluminium (hydr)oxides

Fe- and Al-(hydr)oxides usually have amphoteric surfaces. This means that depending on the pH their surface charge is different and that they can thus adsorb both anions and cations. For a lot of metals and oxyanions the mechanism behind the sorption is inner-sphere complexation, involving ligand exchange (Peacock and Sherman 2004; Sherman and Randall 2003; Arai and Sparks 2001; Arai et al. 2001). The reactive surface area is usually greater for poorly crystalline (hydr)oxides than for more crystalline ones. Fh and amorphous Al hydroxide can exceed a surface area of 600 m<sup>2</sup>g<sup>-1</sup> (Goldberg 2002; Davis and Leckie 1978). With time less crystalline (hydr)oxides undergo gradual crystallization and are thus particularly prevalent in young soils, such as those found in northern Europe that formed after the last glaciation. Since Fh has a remarkably high sorption capacity (Jambor and Dutrizac 1998), it plays a bigger role in Fe mobility than goethite and haematite, even though they are typically more abundant in soils. Al is predominantly found in the form of aluminosilicates, with gibbsite being the only Al hydroxide that occurs in substantial amounts in crystalline form. The less crystalline allophane and imogolite are mainly found in Andosols (Wada 1989) or in spodic horizons of for example Swedish forest soils (Gustafsson et al. 1999; Tiberg 2016).

#### 3.1.1 Ferrihydrite

Fh, a poorly crystalline nanomineral of spherical shape with a grain size of 2-10 nm, is found throughout various soil and aquatic environments and is the most common nano-mineral in soils among all Fe-(hydr)oxides, since it is the most stable form (Hiemstra 2015). Its point of zero charge (PZC) is around pH 8.1 (Mendez and Hiemstra 2020) and it governs the bioavailability and mobility of a variety of cations and anions (Sherman and Randall 2003; Peacock and Sherman 2004). However, its structure is still not completely agreed on (Michel et al. 2010; Michel et al. 2007b; Manceau 2012; Hiemstra 2013). X-ray diffraction (XRD) can differentiate between most common Fh types by the number of peaks present in the XRD pattern. Generally, the smaller, more hydrated, and disordered 2-line (particle size of 1-4 nm) and more crystallised 6-line Fh are the most frequent forms that occur (Cornell and Schwertmann 2003; Michel et al. 2007a). Hiemstra (2013), Hiemstra (2015), and Hiemstra (2018) proposed a new perspective on the surface chemistry of Fh by characterizing the distribution of hydroxyl groups across the nanoparticles using the single-phase model of Michel et al. (2010). In this model Fh ideally comprises three kinds of Fe sites (Fe1, Fe2, Fe3) with Fe1 being 60% hexa-coordinated, Fe2 20% hexa-coordinated and Fe3 20% tetrahedrally coordinated. The structure proposed by Hiemstra (2013) is displayed in Figure 1. One tetrahedral Fe3 can be found in the middle (grey), while two sheets of Fe1 octahedrons that share edges (yellow) are stabilised by three octahedral Fe2 (green). Four different sorts of oxygen atoms can be identified, each of them can be linked to one, two, or three Fe atoms, resulting in a single coordinated corner ('C') and edge ('E') oxo -O (orange), double  $\mu$ -O (blue) or triple  $\mu_3$ -O (black) coordination. Hiemstra (2013) suggested that the low –OH core is defect-free and can be described by Fe<sub>5</sub>O<sub>8</sub>H (Michel et al. 2010) while the -OH groups on the surfaces are more hydrated (Fe<sub>5</sub>O<sub>8</sub>H + nH<sub>2</sub>O) but depleted in Fe<sub>3</sub> tetrahedral and Fe2 octahedral sites. Fe(III) is poorly suitable for a tetrahedron and is thus only stable in the centre of the mineral. Also, Fe2 is implied to be less stable, since it was substantially depleted in a Pair distribution function analysis conducted by Michel et al. (2010). The reduced stability may

result from the asymmetric coordination environment, that is characterised by three unusually short and three unusually long Fe-O bonds. The bond length differs from 24 pm for 2-line Fh to 36 pm for 6-line Fh. For Fe1 the bond difference is only less or equal to 8 pm. The presence of surface groups contribute to a high water content in 2-line Fh, while the mineral core contains only little hydrogen (Hiemstra 2013). This model has been proven to be effective by Boily and Song (2020) in capturing the size-dependent pattern and density of -OH groups. They identified that it is mostly hydrogen-bonded -OH and  $\mu-OH$  groups that are present on the surface of Fe, that the most reactive surface hydroxo-groups are mainly free, and that Fe establishes an intricate H-bond network constructed by less reactive  $\mu-OH$  groups. Nevertheless, the degree to which this is indicative of the actual structure remains uncertain.

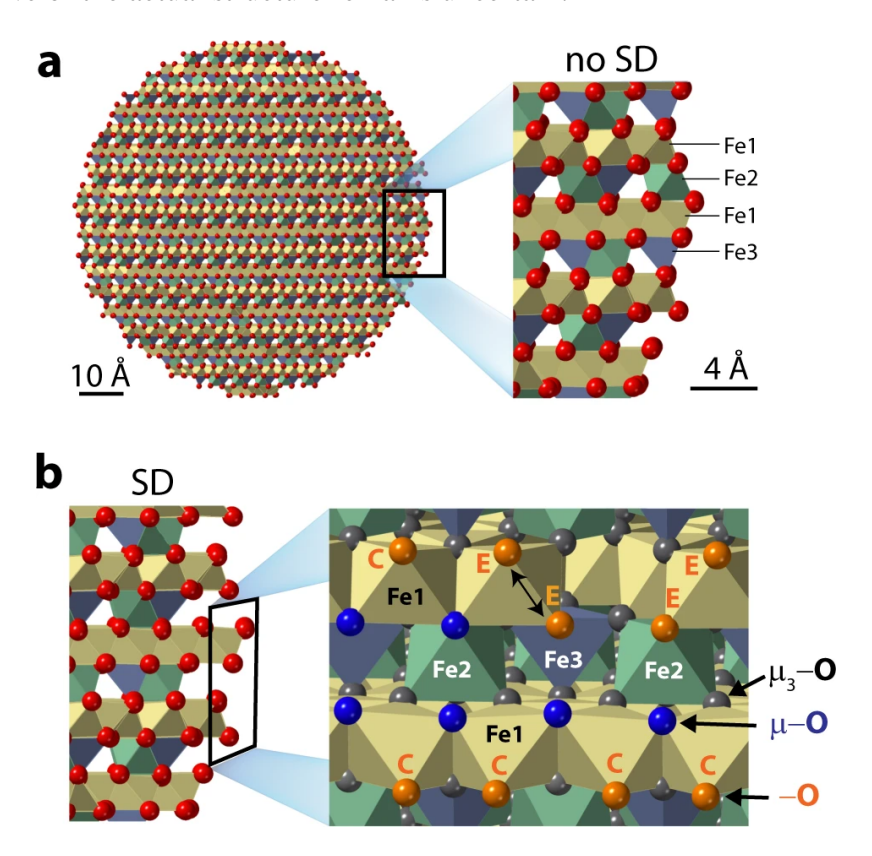


**Figure 1:** Schematic representation of the structure of Fh. a) Spherical Fh nanoparticle (8 nm diameter). The close-up displays no surface depletion (no SD) of Fe2 and Fe3 sites, while b) shows it with surface depletion (SD) (Boily and Song 2020).

The structure results in two types of reactive surface groups,  $\equiv$ FeOH<sup>1/2-</sup> and  $\equiv$ Fe<sub>3</sub>O<sup>1/2-</sup> that can be protonated at low pH values below the PZC to  $\equiv$ FeOH<sub>2</sub><sup>1/2+</sup> and  $\equiv$ Fe<sub>3</sub>OH<sup>1/2+</sup> respectively. During the process of Fe precipitation, Fh is typically the first phase that is developed (Jambor and Dutrizac 1998). It can form from rapid hydrolysis of Fe(III) or rapid oxidation of dissolved Fe(II) to Fe(III) with subsequent precipitation as poorly crystalline nanoparticles. Although Fh is thermodynamically unstable and thus transforms into more stable Fe minerals, such as goethite ( $\alpha$ -FeOOH), haematite ( $\alpha$ -Fe<sub>2</sub>O<sub>3</sub>) or lepidocrocite ( $\gamma$ -FeOOH), adsorption of inorganic and organic molecules can slow this conversion down (Jambor and Dutrizac 1998; Sassi et al. 2021). Additionally, organic acids can partly cover the surface and thus reduce the available sites for sorption (Vermeer et al. 1998).

#### 3.1.2 Imogolite-type Nanoparticles

In older literature often the term imogolite-type materials (ITM) is used, since the particle size was not determined. Here, all materials described as ITM will be referred to as ITN. The term 'ITN' covers allophane, imogolite and their common precursor PIM. Overall, ITNs are important mineral phases in the soil due to their very large surface area (700 m<sup>2</sup>g<sup>-1</sup> to 1500 m<sup>2</sup>g<sup>-1</sup>) and strong capacity to sorb oxyanions (Parfitt 2009).

Allophane is a poorly crystalline aluminosilicate that occurs as spherical particles with diameters between 4 nm and 6 nm and a varying Al:Si ratio between 1 and 2 (Levard and Basile-Doelsch 2016).

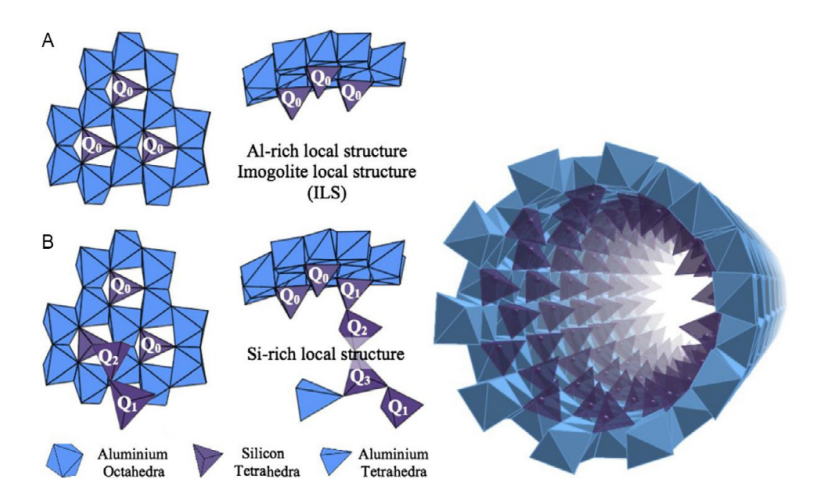


**Figure 2:** Schematic representation of the structure of an imogolite nanotube with A) Al-rich and (B) Si-rich local structure. Si sites are indicated by Qn, n (0-4) is the number of directly linked Si tetrahedrons (Levard and Basile-Doelsch 2016).

Imogolite is an aluminosilicate nanotube with the empirical formula (HO)<sub>3</sub>Al<sub>2</sub>O<sub>3</sub>SiOH that is usually the weathering product of volcanic fragmented rock and is thus widely found in Andosols, but also in many spodic B horizons since it accumulates there due to the podzolisation process (see chapter 3.2) (Gustafsson et al. 2001). It has a porous, fibrous structure that is made up of nanotubes with a diameter of 0.9-2 nm. Imogolite (structure displayed in Figure 2) is characterized by an external curved gibbsite-like layer and orthosilicate anions on the inner surface. The silicon (Si) monomers are connected to six Al atoms. No isomorphic substitution is taking place, but the outer surface of imogolite is composed of doubly coordinated  $\equiv$ Al<sub>2</sub>OH groups that have a weak structural positive charge, although mostly unreactive. This results from steric effects due to the curved structure which leads to a nonsymmetric repartition of the electronic density around Si<sup>4+</sup> and Al<sup>3+</sup> cations, having longer Al-O bond lengths at the outer surface. The inner surface features ≡SiOH groups that tend to develop a negative charge, especially under alkaline conditions (Levard et al. 2012; Gustafsson 2001b). Having this particular arrangement of an isolated silica tetrahedra is very distinctive to the imogolite-structure and is thus called an 'imogolite local structure' (ILS) (Levard et al. 2012). In synthetic imogolite point defects have been reported in the octahedral and tetrahedral layer, but the low zero net charge obtained through calculations indicates that those vacant sites are probably few in natural imogolite (Yucelen et al. 2012). Nevertheless, they are potentially responsible for generating a permanent surface charge, along with the resulting bond undersaturation and proton binding (Fernandez-Martinez and Michot 2016). Gustafsson (2001b) associates the permanent charge with the material's capacity

to sorb anions. Additionally, structural defects and poorly coordinated atoms at the tube ends are commonly cited as alternative explanations for anion adsorption. Also, single coordinated  $\equiv$ AlOH groups are located at the tube edges and at structural defects along the wall. These groups are highly reactive and form strong inner-sphere complexes with oxyanions (Hiemstra and Zhao 2016).

Whereas imogolite is poorly crystalline, PIM is an amorphous precipitate that is regarded as a precursor to imogolite (Levard et al. 2012). PIM has the same local structure and chemical composition and is thus similar to imogolite, but is different in crystallinity. While imogolite is highly ordered in one direction, PIM has no order. PIM lacks a well-formed gibbsite-like sheet and is often characterized by a globular or roof tile-like morphology. Because of electrostatic interactions between negatively charged  $\equiv$ SiOH groups and positively charged  $\equiv$ AlOH groups, the particles can group together and form spherical or tubular structures. As a result, PIM contains a higher number of singly coordinated  $\equiv$ AlOH groups, which makes it significantly more reactive than the tubular form of imogolite (Florén et al. 2025). Those highly reactive ≡AlOH groups have a PZC of around pH 10-11 (Gustafsson 2001b). However, Florén et al. (2025) found three distinct morphologies of PIM: a structureless, amorphous cluster, fragmented nanotubes and globular aggregates. This suggests that the reported structure of PIM may be incomplete so far and that other possible morphologies should be taken into account. Furthermore, Florén et al. (2025) showed by using Fourier transform infrared spectroscopy (FTIR) that PIM, mostly in the form of clusters, dominates over tubular imogolite in the studied Swedish forest soils. The co-existence of both newly formed PIM and polymerised tubular imagolite can be explained by constant formation and dissolution of PIM in natural systems, by for example organic acids released by plants (Kleja et al. 2005; Florén et al. 2025). Also, in the synthetic formation process from PIM to imogolite, Picot et al. (2023) found both PIM and imogolite to occur simultaneously even after prolonged periods and postulated that PIM might never fully grow into tubular nanotubes.

Therefore, since PIM dominates in Swedish Podzols and exhibits much greater reactivity, determining the sorption behaviour of PIM is crucial for understanding the overall reactivity of ITN and building a reliable model.

# 3.2 Phosphorus

Since P is part of a number of essential molecules, like nucleic acids (DNA, RNA), energy transfer molecules (ATP) or within bones and teeth of animals and humans, its bioavailability plays a fundamental role. It needs to be solubilised, so it can be taken up by plants, that require P in a specific stoichiometric ratio to other elements, such as N (Elser and Hamilton 2007).

P can occur in various oxidation states. However, in nature, in its inorganic form, it is mostly present as orthophosphate ions ( $H_2PO_4^-$ ,  $HPO_4^{2-}$ ,  $PO_4^{3-}$ ) with an oxidation state of +V. In soil,  $H_2PO_4^-$  and  $HPO_4^{2-}$  are the most common ionic species within its natural pH range ( $\sim 3$ –10) (Larsen 1967; Hinsinger 2001). In this thesis, P will be used to describe all phosphate species in the soil collectively. Free P concentrations in soil are typically estimated to be between 1  $\mu$ M and 10  $\mu$ M, which lies at the lower end of the optimal range for plant growth (approximately a few to several tens of  $\mu$ M) (Hinsinger 2001).

P availability is affected by its chemical speciation, which changes during ecosystem development (biogeochemical processes of P in soil displayed in Figure 3). Most P in soils is

originally bound within primary minerals, mostly apatite. This P is not available to organisms, but as apatite is weathered, P is released and becomes biogeochemically active (Walker and Syers 1976). In Swedish forests Podzols predominate (Gustafsson et al. 1998). During podzolisation, organic acids, present in acidic surface horizons, cause silica weathering. An illuvial E horizon forms and Fe<sup>3+</sup> and Al<sup>3+</sup> move down to the B horizon. There they precipitate as poorly crystalline mineral phases, mostly as ITN and Fe(III)-(hydr)oxides (Fh and goethite) (Lundström et al. 2000b: Gustafsson et al. 1998). Dissolved P species are retained by those highly adsorbing surfaces (see chapter 3.1.1 and 3.1.2), acting as geochemical buffer, but are thus not readily available to plants. Generally, P can be either sorbed due to ligand exchange between P and OH and OH<sub>2</sub> groups at the surface (inner-sphere complexation) or by surface precipitation of P with Al<sup>3+</sup>, Fe<sup>3+</sup> or at higher pH Ca<sup>2+</sup> ions. Those processes are often summarised together under sorption, irrespective of the mechanism (Dixon and Schulze 2002; Pierzynski et al. 2005; Tuyishime 2022). The strong interaction between P anions and the positively charged soil mineral surfaces might be explained by oxygen (O) being more electronegative than P, wherefore the electron density lies towards the O, giving it a negative charge (Tuyishime 2022). The speciation of P in soil is also influenced by the presence of competing ligands in the soil solution, particularly organic ligands such as citrate and oxalate, which form stable complexes with calcium (Ca), Fe and Al. As a result, P in the soil solution is not limited to orthophosphate ions, but can exist in different forms (neutral, negatively or positively charged). Factors such as soil pH, the availability of metal cations (Ca, Fe, Al) and the presence of organic and inorganic ligands largely determine how these different P species are distributed (Hinsinger 2001).

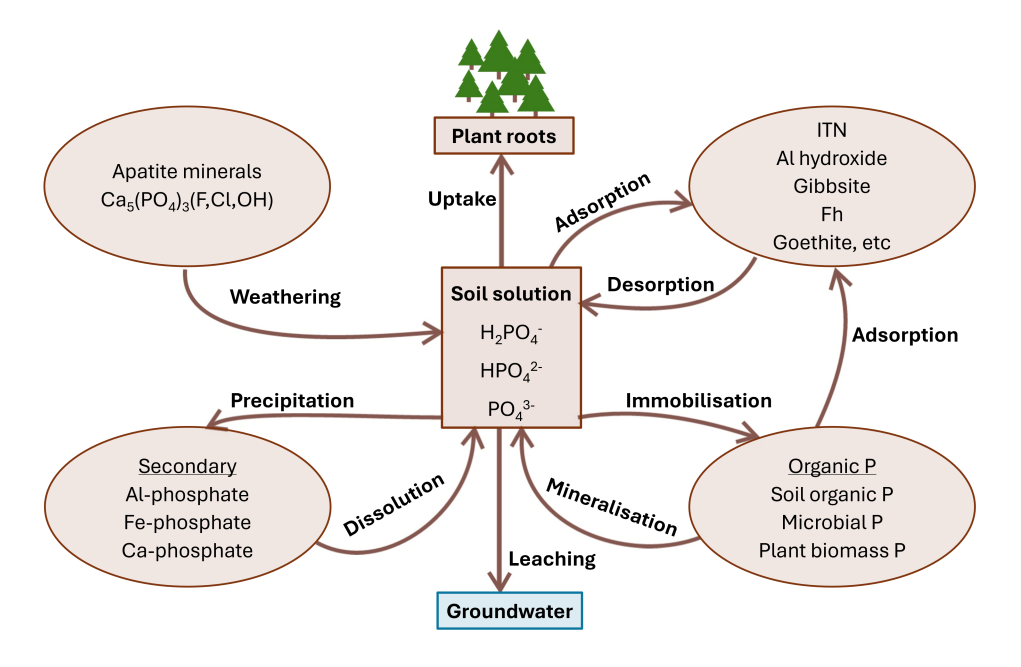


**Figure 3:** Biogeochemical processes of P (Tuyishime 2022).

For Swedish forest soils, Tuyishime et al. (2022) and Tuyishime et al. (2024) found that soil organic P is mainly formed due to the P uptake by plants and microorganisms, which subsequently leads to the development of Oe horizons. Across seven podzolised forest soils the total P stock was  $4.0 \, \mathrm{gm^{-2}}$  in the Oe,  $9.5 \, \mathrm{gm^{-2}}$  in the A and E horizons,  $117.5 \, \mathrm{gm^{-2}}$  in the B and  $109.3 \, \mathrm{gm^{-2}}$  in the C horizon. However, the P that was translocated into the B horizon was adsorbed by 58%, mainly to Al- and Fe-phases with ITN being the most important sorbent surface. Furthermore, they hypothesize that also organic P contributes to the Fe- and Al-bound P pool and that the ratio of P:Fe and P:Al on the oxide surfaces might influence the plant uptake of P (Tuyishime et al. 2022).

Thus, the B horizon of Podzols stores large amounts of P. However, the question to what extent P bound to Fe- and Al-(hydr)oxides is actually available to plants is still debated (Klotzbücher et al. 2020; Jones and Oburger 2011). Plants, bacteria and fungi can for example mobilize P from mineral surfaces, making it available for plant absorption (Schreider et al. 2022; Jones and Oburger 2011).

# 3.3 P-Solubilising Mechanisms

Many plant species have adapted to environments with limited P availability by developing various strategies that enhance their capacity to receive P from the soil. Microorganisms can contribute to the dissolution of P making it available for plant uptake in acidic forest soils, where the P supply is limited. They can release complexing or mineral dissolving compounds like organic acid anions, siderophores or protons, extracellular enzymes or they deliver organic P during substrate degradation (Jones and Oburger 2011). Thus, a lot of plants undergo symbiosis with ectomycorrhizal fungi (EMF) to obtain P and other nutrients through the fungal mycelium, while the fungi in exchange get photosynthates (Jansa et al. 2011; D'Amico et al. 2020). This increases enzyme activity (Plassard et al. 2011), secondary metabolites production (Shah et al. 2015) and greater water uptake during drought (Courty et al. 2010) and hence leads to even better P uptake (D'Amico et al. 2020). Studies show that in P-deficient soils more EMF grow because the plant releases more carbon (C) to the fungal symbionts in the search for P (Almeida 2019). EMFs can release organic acids, polyphenols, phosphatases, siderophores or exopolysaccharides (Landeweert et al. 2001). The organic acid anions compete with P for the same binding sites on mineral surfaces via ligand exchange or complex metal cations that are part of P sorption. Also, by decreasing the pH of the soil solution, organic acids can dissolve minerals, setting P free. Polyphenolic compounds, which provide electrons, can dissolve reductive Fe-oxides, and phosphatases can make organic P accessible (Rosling 2009; Shah et al. 2015; D'Amico et al. 2020). Furthermore, D'Amico et al. (2020) proposed that P adsorbed onto mineral surfaces was directly released by EMF activity, since they found fungal growth on the mineral surfaces. Andrino et al. (2019) discovered that arbuscular mycorrhiza in symbiosis with tomato effectively liberate P and phytate bound to goethite. Merlin et al. (2016) suggested that the found uptake of P associated with goethite or amorphous Al-oxide by palisade grass and ruzigrass was potentially because of organic acids and enzymes that were liberated by plants.

Organic acids present in the soil solution comprise humic acids ( $> 3000\,\mathrm{Da}$ ), fulvic acids ( $1000\text{-}3000\,\mathrm{Da}$ ), and low molecular weight organic acids (LMWOA;  $< 1000\,\mathrm{Da}$ ). LMWOAs are characterised by having at least one carboxyl group and can thus be negatively charged. Depending on the number of carboxyl groups, as well as their distribution, all organic anions have a particular speciation profile as a function of soil solution pH. Their protonation constants ( $pK_a$ ) indicate the pH when 50% of the carboxyl groups are protonated while the other half is present as the carboxylate anions (Sokolova 2020; Jones and Brassington 1998). Their sorption to solid surfaces allows for the mobilisation of other adsorbed nutrients, such as P for plant uptake. The fate of LMWOAs in soil is complex, due to various interactions, depending on the species present (Jones 1998). Figure 4 schematically displays important fluxes and pools.

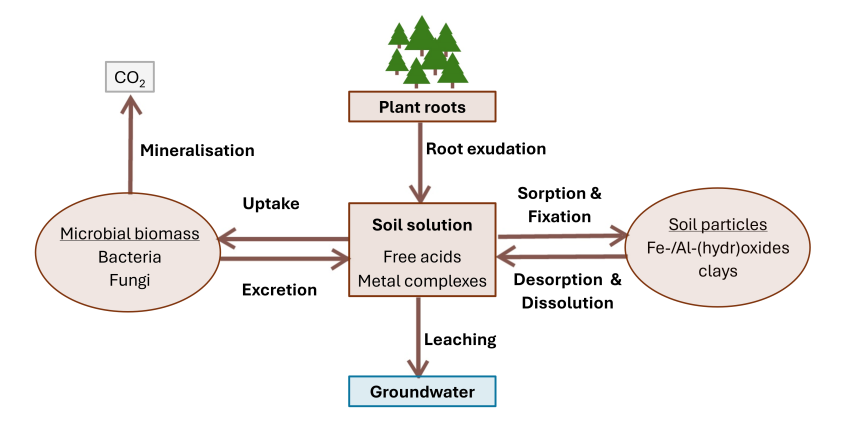


Figure 4: Important fluxes and pools of LMWOAs (Jones 1998).

Plants growing on podzol soils have been found to secrete LMWOAs, and this process is encouraged by their symbiotic relationship with mycorrhizal fungi (Lundström et al. 2000a; Sokolova 2020). LMWOAs in the soil solution of forest ecosystems include aliphatic acids, particularly oxalic, malic and citric acid, as well as aromatic acids, of which unsubstituted benzoic and cinnamic acid predominate (Sokolova 2020). In Norway spruce and deciduous trees, malic and citric acid were reported to be the most abundant of low molecular weight (LMW) aliphatic acids in litter extracts (Nykvist 1963). Fox and Comerford (1990) observed oxalic, formic and citric acid in the forest floor in the US and oxalic acid was also found in the soil solution of ectomy-corrhizal hyphal plants in a concentration of 7 mM (Griffiths et al. 1994). Furthermore, Balland et al. (2010) showed that bacterial strains isolated from Podzol horizons also release gluconic acid.

The concentration of LMWOAs in plant tissues, root exudates and microbial metabolites ranges from several to tens of mM, but is one or two orders of magnitude lower in the bulk soil solution (about  $0.1\text{-}100\,\mu\text{M}$ ) due to dilution, biodegradation and sorption onto the solid phase (Sokolova 2020; Jones 1998). Furthermore, the concentration declines with depth. In a study conducted by Lundström et al. (2000b) with three coniferous forest soils, only oxalic, shikimic and sometimes citric acid were found in the B horizon. Nevertheless, in the microbial, hyphal and root micro-environment the concentration of LMWOAs can be locally greatly increased (Landeweert et al. 2001). LMWOAs diffuse from the root cytosol to the surrounding soil solution along the concentration gradient or via the electrochemical potential on the cytoplasmic membrane (Jones 1998).

Therefore, in this thesis, LMWOAs present in the soil were evaluated according to their ability to set P adsorbed onto Fh and ITN free. The organic acids of choice were *D*-gluconic and oxalic acid since both are secreted by plant roots and mycorrhizal hyphae (Sokolova 2020; Balland et al. 2010; Landeweert et al. 2001; Lundström et al. 2000b) and have been reported in literature before. Their structure and protonation constants can be seen in Table 1. For oxalic acid, Bhatti et al. (1998) could show that it successfully competed with P for sorption sites in the spodic horizons of Spodosols with Fe- and Al-(hydr)oxides present.

<b>Table 1.</b> Suluctures and individuation constants for oxalle and 17-2 fuctine acid.	Table 1: Structures and	protonation constants	for oxalic and a	D-gluconic acid.
--	-------------------------	-----------------------	------------------	------------------

Organic acid	Acid Anion Abbreviation	Structure	$pK_{a1}^a$	$pK_{a2}^a$
D-Gluconic acid	GL	HO OH OH OH OH OH	3.6	
Oxalic acid	Ox	НО ООН	4.4	1.46

 $<sup>^</sup>a$  p $K_a$ -Constants are for 25 °C (ECHA 2025) and will therefore vary slightly for conditions at 8 °C.

# 3.4 Geochemical Modelling

Geochemical modelling improves our understanding of both natural and man-made systems by allowing us to simulate a wide range of chemical reactions and processes. It makes use of mathematical equations that describe the chemistry behind prevalent processes in environmental or geological systems. The number of published papers using geochemical modelling has been rising since 1995 (Khalidy and Santos 2021). There are plenty of free and commercial software tools available, each of them having different strengths and limitations, depending on the specific geochemical processes they are supposed to simulate (Zhu and Anderson 2002; Khalidy and Santos 2021). PHREEQC (Parkhurst and Appelo 2013), Visual MINTEQ (Gustafsson 2024b) and The Geochemists Workbench (Bethke and Yeakel 2009) are most frequently used. They make use of associated databases that contain the information on the species, mineral properties and thermodynamic constants needed. Depending on the complexity, it can be distinguished between four groups of simulated processes. Equilibrium modelling regarding speciation and solubility is the most basic since it does not account for changes over time or space. It is commonly used to assess the saturation of minerals in a solution and to determine the concentration and distribution of dissolved chemical species. Reaction path modelling simulates the evolution of equilibrium states, quantifying the mass transfer between different phases within a system that may be subject to temperature or pressure changes. A mass balance approach, which analyses the transformation between known initial and final aqueous compositions along a flow path, is also used in inverse modelling. The most complex type is reactive transport modelling, which identifies compositional alterations in a moving solution caused by advection and diffusion with passing solids (Zhu and Anderson 2002; Bundschuh and Zilberbrand 2011; Khalidy and Santos 2021).

Visual MINTEQ is used in this thesis. It is a free chemical equilibrium modelling program designed to simulate metal speciation, solubility equilibria, sorption and related processes in natural water systems. Originally developed as a Windows-based version of the DOS program MINTEQA2 (version 4.0), it was released by the U.S. Environmental Protection Agency (EPA) in 1999 and later updated by Gustafsson (Gustafsson 2024a). Different surface complexation models are integrated in the Visual MINTEQ programme to model ion adsorption at solid-liquid interfaces. These models differ in their approach to represent the electrical double layer and

surface reactions (Hiemstra and Van Riemsdijk 1996).

The basic Stern (BS) model (Noh and Schwarz 1989) considers ions to be point charges. It divides the double layer into two regions, a compact charge-free Stern layer and a diffuse double layer. This phenomenon occurs because the surface charge of minerals is counterbalanced by electrolyte ions within the diffuse double layer depending on the pH of the solution. The hydration shell of the ions leads to a certain minimum distance from the charged surface, resulting in the charge-free Stern layer. When this layer is treated as a continuous medium, the concept of electrostatic capacitance can describe how much electric charge is stored. The capacitance value depends on the thickness of the layer and the dielectric constant of the layer. There is an electrostatic plane at each end of the Stern layer. In the plane towards the surface, called  $\theta$ -plane, protons that adsorb to the surface are located. The so-called  $\theta$ -plane is found between the Stern layer and diffuse double layer. That is where outer-sphere complexes are found. They sorb through electrostatic interactions via an O or H<sub>2</sub>O ligand to the surface (Hiemstra and Van Riemsdijk 1996; van Riemsdijk and Hiemstra 2006).

The three-plane model incorporates a third electrostatic plane to provide a more accurate description of inner-sphere complexes. Inner-sphere complexes are covalently bound to the surface through ligand exchange. Therefore, they are positioned closer to the surface than outer-sphere complexes, resulting in charge within the Stern layer. This charge is located in the so called I-plane, dividing the Stern layer into two charge-free layers, giving them two different capacitance (Hiemstra and Van Riemsdijk 1996). The location of inner-sphere and outer-sphere complexes using  $PO_4^{3-}$  as example is schematically shown in Figure 5.

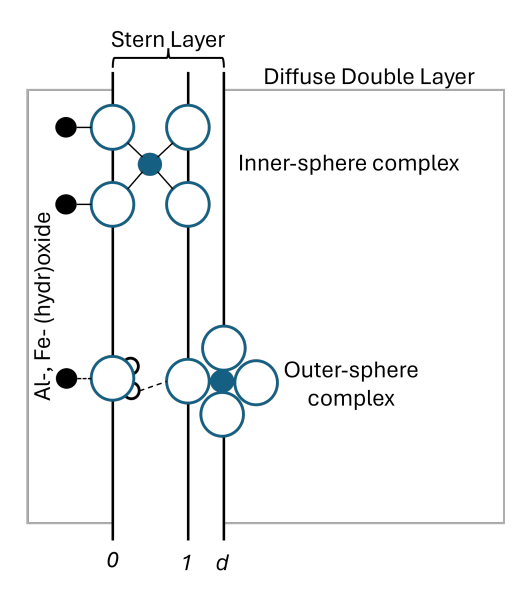


**Figure 5:** Scheme of the location of inner- and outer-sphere complexes of PO<sub>4</sub><sup>3-</sup>. White circles represent O, blue circles P, black circles Fe/Al, small white circles H. Plane *1* dividing the Stern layer is not described in the BS model. Adapted from Hiemstra and Van Riemsdijk (1996).

The CD-MUSIC (Charge distribution multisite complexation) model builds on the three-plane model but additionally uses the Pauling bond valence concept (Pauling 1929) to describe the distribution of charge within surface complexes instead of treating them as point charges (Hiemstra and Van Riemsdijk 1996).

Modelling experimental findings will improve our understanding of future P availability. It can predict potential deficiencies and identify when sufficient P is present. Consequently, it can reduce fertiliser use and prevent eutrophication.

# 4 Material and Methods

# 4.1 Equipment

#### **General methods**

Reagents were purchased from different commercial sources and used without further purification. All used tubes and glassware were acid washed in  $0.1\,M$  HNO $_3$  overnight and run through the dishwasher to remove all potential residues stuck on the surface. All experiments were carried out using MilliQ water (18.2 M $\Omega$  cm) obtained from ELGA purification systems.

#### Determining the pH

The pH was measured using a Radiometer PHM93 pH meter equipped with a combination electrode (Radiometer Analytical SAS, Lyon, France).

#### Centrifuge

Samples were centrifuged with an Allegra X-15R Centrifuge (Beckman Coulter©, Inc. in the United States and other countries).

#### **DOC-Analysis**

The dissolved organic carbon (DOC) was determined with a TOC/TNb analyser (Multi N/C 2100S, analytikjena, Jena, Germany). Samples were thawed a day prior to analysis. Samples were analysed in a 24 h automatic run. Samples were thus exposed to room temperature up to 20 h before analysis. A standard series, containing a known concentration of inorganic carbon (IC) (1 mg IC/mL, 2 mg IC/mL, 4 mg IC/mL, 10 mg IC/mL and 20 mg IC/mL) was prepared to account for the instrument's accuracy. From the measurement of IC and total carbon (TC), the total organic carbon (TOC) is calculated. Since all samples were filtered prior to analysis, TOC is equivalent to DOC.

#### **ICP-OES Analysis**

The amount of dissolved P, Fe, Al and Si was measured at Royal Institute of Technology (KTH) in Stockholm with inductively coupled plasma optical emission spectroscopy (ICP-OES, Thermo Scientific iCAP 6000 Series). Samples were thawed a day prior to analysis and 10 mL of the undiluted sample acidified with 0.15 mL of concentrated HNO<sub>3</sub> (65%) to end up with 1 % HNO<sub>3</sub> to make sure all components were dissolved. A standard series of known concentrations of P, Fe, Al and Si was prepared, using the same background as in the samples (10 mM NaNO<sub>3</sub>, 1 % HNO<sub>3</sub>). Through linear regression, the concentration of the standard series was determined giving the calibration curve. The software compares the intensity of each peak with the calibration standards to calculate concentrations. Every eight samples, the blank and the highest standard were measured again to account for the instrument's drift. The values in-between were interpolated according to the slope before and after the measured samples, as well as the value of the interpolated blank deducted.

# 4.2 Overview of the Experimental Work

P adsorption as a function of pH, as well as the influence of *D*-gluconate (GL) and oxalate (Ox) on the P adsorption was studied for two different particles, present in the B horizon of Swedish Podzols, namely Fh and PIM. Five different batch series for each mineral were carried out. A graphical abstract can be seen in Figure 6.

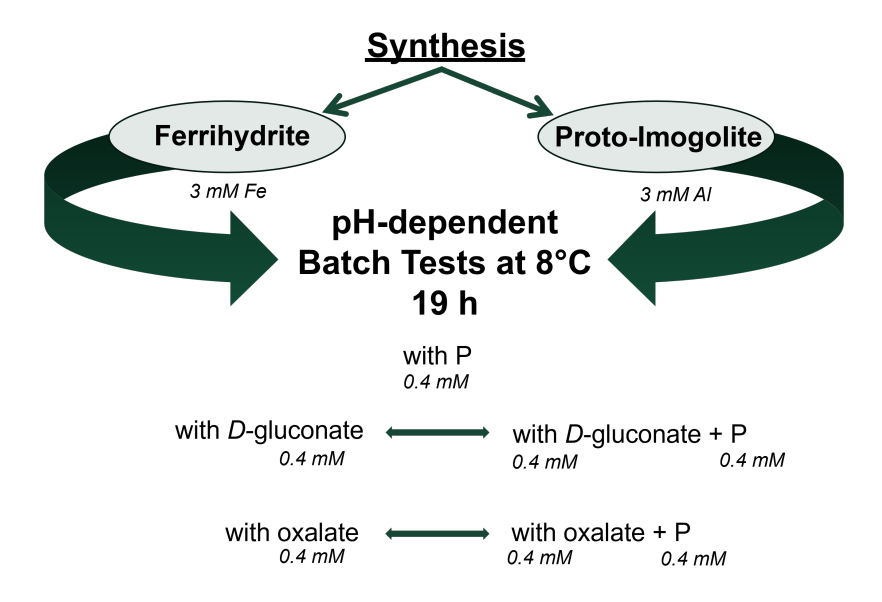


Figure 6: Graphical abstract of the experimental work.

# 4.3 Experimental Procedures

## 4.3.1 Synthesis of Ferrihydrite

Fh was synthesised similarly to Hiemstra and Zhao (2016) and as stated earlier by the research group (Tiberg et al. 2013; Gustafsson 2003). Under stirring, a 4 M NaOH (10 mL) solution was added dropwise to a 500 mL orange solution of  $Fe(NO_3)_3 \cdot 9 \, H_2O$  (7.277 g, 36 mM), NaNO<sub>3</sub> (0.515 g, 12 mM) and MilliQ water until the pH was relatively stable at 8.0. After the brown suspension was standing for 21 h, a 0.1 M HNO<sub>3</sub> (15 mL) solution was added dropwise under stirring till a pH of 4.6. The suspension was stirred for 1 h (to avoid excessive  $CO_2$  in the suspensions) and Fh was obtained as a suspension of brown particles and stored in the fridge up to one month.

Since it has been confirmed that the Fe(III)-oxide, synthesised after this procedure, consists of 2-line Fh and the research group has always obtained Fh, no further analysis was carried out. The specific surface area (SSA) has been estimated to be  $611 \, \text{m}^2 \text{g}^{-1}$  (Hiemstra and Zhao 2016).

# 4.3.2 Synthesis of Proto-Imogolite

PIM was synthesised following the procedure of Farmer et al. (1983), that was adapted by Ohashi et al. (2004) and Adams et al. (2024). An AlCl<sub>3</sub> solution was prepared in a 100 mL flask from AlCl<sub>3</sub>  $\cdot$  6 H<sub>2</sub>O (6.766 g, 280 mM), as well as 100 mL of Na<sub>2</sub>SiO<sub>2</sub> solution (4.4 mL, 280 mM). To get an Al:Si ratio of 2:1, 40 mL of the 280 mM Na<sub>2</sub>SiO<sub>2</sub> solution were added to 80 mL of the

280 mM AlCl<sub>3</sub> solution under slow stirring, resulting in 186 mM total Al and 93 mM total Si and a pH of 3.15. 160 mL of a 280 mM NaOH solution was added dropwise using a peristaltic pump at a rate of 1 mLmin<sup>-1</sup> under slow stirring, giving a OH:Al:Si ratio of 2:1:0.5 (160 mM NaOH, 80 mM Al, 40 mM Si, respectively) with a pH of 4.2. The reaction mixture was stirred at 400 rpm for 1 h at room temperature and transferred to anaerobic glass bottles. The anaerobic glass bottles were placed in a water bath of 95 °C for 2-3 days. After cooling down to room temperature, a 1 M NaOH solution (10 mL) was added dropwise to adjust the pH from 3.6 to 4.8. The white suspension was transferred into dialysis tubes and placed in MilliQ water for 3 days. The MilliQ water was exchanged after one day. PIM was obtained as a white suspension and stored in the fridge for up to one month.

#### 4.3.3 Batch Experiments with Ferrihydrite

The background electrolyte of all suspensions was  $0.01 \, M$  NaNO<sub>3</sub>. Polypropylene centrifuge bottles were prepared ending up with a total volume of  $40 \, \text{mL}$ . The concentration of Fh suspension was fixed at 3 mM total Fe (3.41 mL Fh suspension). Different amounts of  $4 \, \text{mM}$  HNO<sub>3</sub> and  $4 \, \text{mM}$  NaOH were added to produce a range of pH values between pH 3 and 8. In the batch series containing P, to each sample,  $4 \, \text{mL}$  of a  $4 \, \text{mM}$  NaH<sub>2</sub>PO<sub>4</sub>  $\cdot 2 \, \text{H}_2\text{O}$  solution were added at room temperature resulting in  $400 \, \mu\text{M}$  P. The samples were cooled down for  $2 \, \text{h}$  at  $8 \, ^{\circ}\text{C}$  before at  $8 \, ^{\circ}\text{C}$  either  $4 \, \text{mL}$  of a  $4 \, \text{mM}$  NaC<sub>6</sub>H<sub>11</sub>O<sub>7</sub> solution in the series of GL, or  $4 \, \text{mL}$  of a  $4 \, \text{mM}$  Na<sub>2</sub>C<sub>2</sub>O<sub>4</sub> solution in the series of Ox were added, ending with a concentration of either  $400 \, \mu\text{M}$  GL or  $400 \, \mu\text{M}$  Ox. All treatments were duplicated. The samples were shaken for  $19 \, \text{h}$  at  $8 \, ^{\circ}\text{C}$  on an over-end shaker. They were centrifuged for  $20 \, \text{min}$  with  $3000 \, \text{rpm}$  at  $8 \, ^{\circ}\text{C}$  and filtered using  $0.2 \, \mu\text{m}$  single-use Acrodisc PF filters (Pall Corporation, Ann Arbor, MI, USA). The pH was measured on unfiltered samples. The filtered samples were frozen to avoid any possible decomposition. Samples were thawed a day prior to analysis of DOC and P, Fe.

# 4.3.4 Batch Experiments with Proto-Imogolite

Polypropylene centrifuge bottles were prepared ending up with a total volume of 40 mL. The background electrolyte of all suspensions was 0.01 M NaNO3. The concentration of PIM suspension was fixed at 3 mM Al. Different amounts of 4 mM HNO3 and 4 mM NaOH were added to produce a range of pH values between pH 3 and 8. In the batch series containing P, to each sample, 4 mL of a 4 mM NaH2PO4  $\cdot$  2 H2O solution were added at room temperature resulting in 400  $\mu$ M P. The samples were cooled down for 2 h at 8 °C before at 8 °C 1.5 mL of PIM and either 4 mL of a 4 mM NaC6H11O7 solution in the series of GL, or 4 mL of a 4 mM Na2C2O4 solution in the series of Ox were added ending with a concentration of either 400  $\mu$ M GL or 400  $\mu$ M Ox. All treatments were duplicated. The samples were shaken for 19 h at 8 °C on an over-end shaker. They were filtered through centrifugation (3500 rpm, 15 min, 8 °C) in 10K MWCO Centrifugal Devices (Pall Corporation, Ann Arbor, MI, USA). The filters were rinsed once with MilliQ water in the centrifuge prior to use. The pH was measured on unfiltered samples. The filtered samples were frozen and a day prior to analysis of DOC and P, Al, Si thawed.

# 4.4 Modelling with Visual MINTEQ

Surface complexation modelling for Fh was performed with the CD-MUSIC model (Hiemstra and Van Riemsdijk 1996) in Visual MINTEQ 4.0 (Gustafsson 2024b)) which uses the Three-Plane interface model. The updated version from Gustafsson and Antelo (2022) was used. Sites are divided into singly ( $\equiv$ FeOH<sup>1/2-</sup>) and triply coordinated ( $\equiv$ Fe<sub>3</sub>O<sup>1/2-</sup>) groups, in which the former are further subdivided into groups that can either coordinate corner-sharing (indicated with a small e) or edge-sharing (indicated with a small e) bidentate complexes (Table 2). Furthermore, they can be split into sites of high-affinity (indicated with a small h in brackets). However, those high-affinity sites seem to mostly play a significant role in cation sorption (Gustafsson and Antelo 2022). Therefore, for anion sorption, high-affinity sites were always tied with the sites of regular affinity. While the singly coordinated groups can also form inner-sphere monodentate complexes, triply coordinated groups only form outer-sphere complexes. Present sites and their respective site densities are found in Table 2. Unless otherwise stated, the SSA was 611 m<sup>2</sup>g<sup>-1</sup>, the inner capacitance 1.1439 Fm<sup>-2</sup> and the outer capacitance 0.8978 Fm<sup>-2</sup>.

**Table 2:** Sites in the Fh CD-MUSIC Model (Gustafsson and Antelo 2022). A small *c* denotes corner-sharing complexes, a small *e* edge-sharing complexes, and a small h in brackets high-affinity sites.

site	site density (sites nm <sup>-2</sup> )
≡FeO <i>e</i> H	2.942
$\equiv$ FeOeH (h)	0.0522
$\equiv$ FeOeH (hh)	0.0058
$\equiv$ FeO $c$ H	2.742
$\equiv$ FeO $c$ H (h)	0.058
$\equiv Fe_3O$	1.4

An unpublished model based on the findings of Florén et al. (2025) was used in order to model the sorption behaviour to PIM. It uses the Basic Stern model and includes  $\equiv$ AlOH as the only reactive site, with a site density of 8.1 nm<sup>-2</sup>, a SSA of 450 m<sup>2</sup>g<sup>-1</sup> and an inner capacitance of 1.2 Fm<sup>-2</sup>.

It was assumed that the concentration of sodium ions (Na<sup>+</sup>) and nitrate ions (NO<sub>3</sub><sup>-</sup>) were the same in the minerals suspension, ending up with a ionic strength of 0.01 M. However, it was accounted for any extra HNO<sub>3</sub> or NaOH that was added in each sample in the batch experiment. The total input of Fh or PIM was corrected according to the amount of Fe or Al dissolved, especially at low pH. Visual MINTEQ corrects activities with the Davies equation. Since dissolved Fe, Al and Si content was not measured in all samples due to time restraints, values were interpolated where possible. For the series of Fh+GL, Fe values were extrapolated for the low pH range. In the series of PIM+GL and PIM+Ox, Si was determined via the interpolated Al:Si ratio from ratios at similar pH of PIM+P+GL and PIM+P+Ox respectively. Negative values in PIM+P+Ox were excluded.

Surface complexation constants for single sorbent systems were optimised with PEST (Doherty 2010), other than for the Fh+P system, as it has been studied in detail by Gustafsson and Antelo (2022). PEST is an included tool in Visual MINTEQ, that uses the Gauss–Marquardt–Levenberg method to adjust the parameters, minimising the weighted sum of the squares of the differences between the model's predicted and the actual experimental values. The fitting variable was the

respective percentage of species adsorbed. Different combinations of CD values in the  $\theta$  and  $\theta$  plane were tested to end up with the best goodness of fit value  $\theta$  for the surface complexation constants. The optimised model parameters (Table 3) were then applied within the competitive systems.

**Table 3:** Best-fit results for surface complexation reactions.

ion	surface complex <sup>a</sup>	no. of H <sup>+</sup> <sub>b</sub> in the reaction	$(\Delta z_0, \Delta z_1)^c$	$\log K^d$	PEST R <sup>e</sup>
	Ferrihydri	te (Fh CD-MUSIC	C Model) <sup>f</sup>		
$PO_4^{3-}$	$\equiv$ FeOPO(OH) <sub>2</sub> <sup>1/2-</sup>	3	(0.4, -0.4)	30.32	
	$\equiv$ FeOPO <sub>2</sub> OH <sup>1 1/2-</sup>	2	(0.35, -1.35)	26.62	
	$\equiv$ FeOPO <sub>3</sub> <sup>2 1/2-</sup>	1	(0.25, -2.25)	18.00	
	$(\equiv \text{FeO}c)_2 \text{POOH}^-$	3	(0.65, -0.65)	33.19	
	$(\equiv \text{FeO}c)_2 \text{PO}_2^{2-}$	2	(0.46, -1.46)	27.93	
RCOO-	$\equiv$ FeOH <sub>2</sub> <sup>1/2+</sup> ····OOCR <sup>-</sup>	1	(0.8, -0.8)	$10.49 \pm 0.20$	0.961
$(R = C_5 H_{11} O_5)$	$\equiv Fe_3OH^{1/2+}\cdots OOCR^-$	1	(0.8, -0.8)	$10.49\pm0.20$	0.961
$C_2O_4{}^{2-}$	$(\equiv \text{FeO}e)_2\text{C}_2\text{O}_2^-$	2	(0.1, -0.1)	$17.42\pm0.07$	0.990
Proto-Imogolite (Basic Stern Model)					
$PO_4^{3-}$	$(\equiv AlO)_2PO_2^{2-}$	2	(0.46, -1.46)	$28.16 \pm 0.65$	0.954
	(≡AlO) <sub>2</sub> POOH <sup>-</sup>	3	(0.45, -0.45)	$34.24 \pm 0.21$	0.954
$RCOO^{-}$ $(R = C_5H_{11}O_5)$	$\equiv$ AlOH <sub>2</sub> <sup>1/2+</sup> ····OOCR <sup>-</sup>	1	(1, -1)	$11.94 \pm 0.21$	0.322
$C_2O_4{}^{2-}$	$\equiv AlOH_2{}^{1/2+}\cdots C_2O_2{}^{2-}$	1	(0.8, -1.8)	$13.11\pm0.28$	0.860

<sup>&</sup>lt;sup>a</sup> High-affinity sites were tied with low-affinity sites. The CD-factors, log K and R values are therefore the same and not displayed separately.

<sup>&</sup>lt;sup>b</sup> Proton stoichiometry in the surface complexation reaction based on  $\equiv$ FeOH<sup>1/2-</sup> as the surface component.

<sup>&</sup>lt;sup>c</sup> CD factors, representing the change of charge in the 0 ( $\Delta z_0$ ) and 1 ( $\Delta z_1$ ) plane.

<sup>&</sup>lt;sup>d</sup> Surface complexation constant with the 95% confidence intervals given by PEST. If no interval is given, log K is either taken from literature or constant and was not fitted during optimisation.

<sup>&</sup>lt;sup>e</sup> The goodness-of-fit parameter given by PEST.

<sup>&</sup>lt;sup>f</sup> Data source for CD factors and log K values for the PO<sub>4</sub><sup>3-</sup> ion is from Gustafsson and Antelo (2022).

# 5 Results and Discussion

# 5.1 Experimental Results

#### 5.1.1 P Sorption in the Single Sorbent Systems

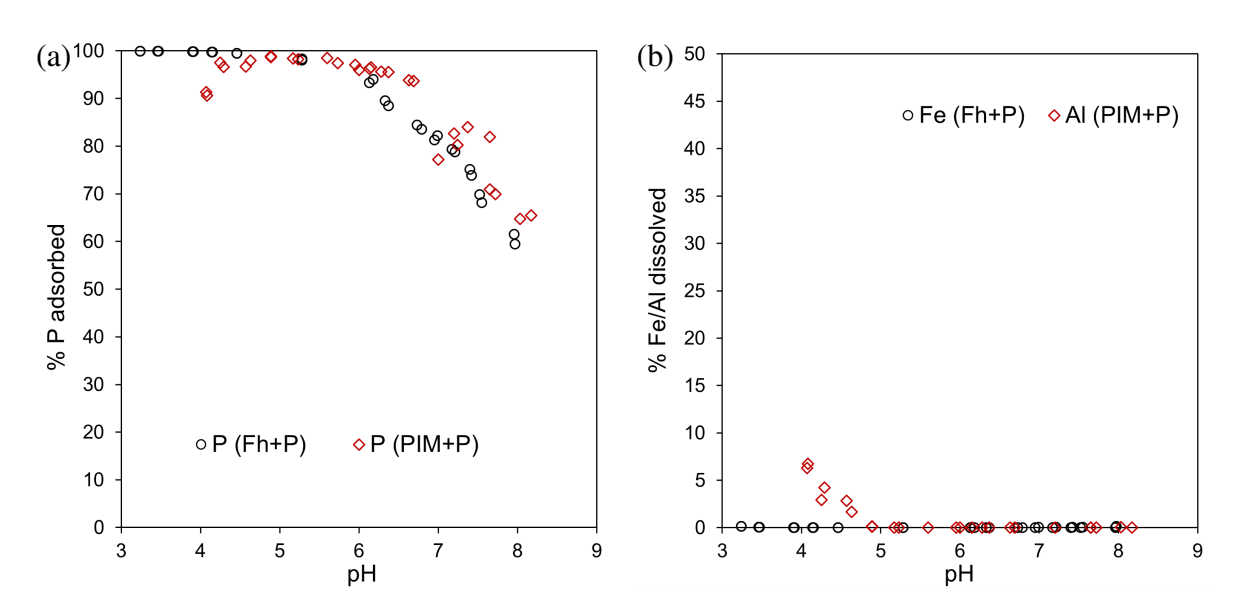


**Figure 7:** a) Phosphorus sorption and b) dissolved Fe and Al as a function of pH in the single sorbent systems. Empty black circles represent data for the series Fh+P, empty red diamonds for the series PIM+P.

Overall, P sorption to both mineral surfaces, Fh and PIM, is high for the studied concentrations between percentages of 60 and nearly 100. P sorption decreases with an increasing pH (Figure 7a). At low pH the surface groups  $\equiv$ FeOH<sup>1/2-</sup>,  $\equiv$ Fe<sub>3</sub>O<sup>1/2-</sup> and  $\equiv$ AlOH<sup>1/2-</sup> become positively charged due to the uptake of one H<sup>+</sup> resulting in  $\equiv$ FeOH<sub>2</sub><sup>1/2+</sup>,  $\equiv$ Fe<sub>3</sub>OH<sup>1/2+</sup> and  $\equiv$ AlOH<sub>2</sub><sup>1/2+</sup> respectively. A higher pH means fewer H<sup>+</sup> ions, thus decreasing the amount of positively charged surface groups leading to a weaker sorption capacity of P anions.

As hypothesised, above pH 5.5, P sorbs more strongly to PIM than to Fh (between 2% and 10% more sorption). This is consistent with previous findings that also allophane sorbs more P than Fh does (Parfitt 1989). This was formerly explained by the formation of amorphous Al-P precipitates, as well as P having higher intrinsic adsorption constants for Al-(hydr)oxides than for Fe-(hydr)oxides in surface complexation reactions. P sorbed to Al-(hydr)oxides seems to be more stable than P sorbed to Fe-(hydr)oxides (Gustafsson 2001a; Uchida et al. 2022; Johnson et al. 2002). Furthermore, this observation is attributed here to the higher SSA of PIM compared to Fh, which gives PIM more available binding sites for P sorption.

Below pH 5.5, P was found to bind with equal strength to Fh and PIM, until at pH 4.9 P sorption to PIM decreases towards lower pH values, while P sorption to Fh stays at nearly 100%. This is due to partial dissolution of PIM at low pH values (Florén et al. 2025). This can be seen in Figure 7b, where the amount of dissolved Al and Fe is shown. Dissolved Fe stays at 0%, throughout the pH range (3–8), suggesting that Fh is stable under the experimental conditions. Dissolved Al increases with decreasing pH from pH 4.9, where only 0.1% Al is dissolved up to

6.3% at pH 4.1 indicating that PIM is dissolving. This results in fewer available surface groups on PIM leading to a decrease in P sorption.

Nevertheless, some of the dissolved Al might also be attributed to dissolved Al from other Al phases that were possibly produced as side product during PIM synthesis or some unreacted Al(OH)<sub>3</sub>. Only slight variations in synthesis conditions, such as the ratio of Al:Si:OH or the rate of NaOH addition can give a mixture of different side products such as imogolite, amorphous silica or pseudo-boehmite  $\gamma$ -AlOOH (Adams et al. 2024). This also explains why the ratio of dissolved Al:Si is not constant (Figure 8). At low pH relatively more Al is dissolved compared to a lower Al:Si ratio at higher pH. This stoichiometric difference is also attributed to the formation of amorphous silica after the release of SiO tetrahedra (Wang et al. 2020).

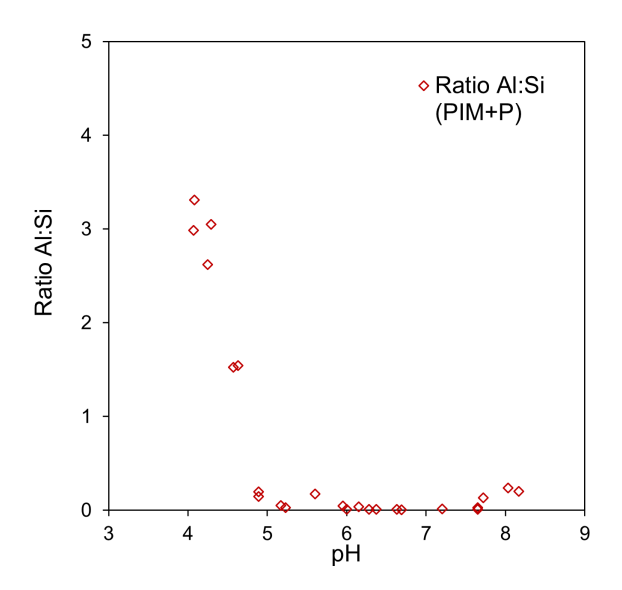


**Figure 8:** Dissolved Al:Si ratio as a function of pH in the system PIM+P.

While the stronger P sorption to PIM than to Fh certainly plays a role, the higher proportion of P bound to Al-(hydr)oxides, as determined by Tuyishime et al. (2022) and Tuyishime et al. (2024) in Swedish forest soils, might mostly be explained by the greater abundance of PIM compared to Fh (Florén et al. 2025), as well as possibly different SSAs of Fh and PIM present in the soil. Due to aggregation, the SSA of Fh could for example be lower relative to the SSA of PIM, binding less P. This again shows the relevance of PIM and the importance of studying its sorption behaviour.

## 5.1.2 Difference in Acid Sorption

Both Fh and PIM exhibited a stronger affinity for P than for the acid anions GL and Ox (compare Figure 7a with Figure 9a,b). For Fh and other Fe- and Al-(hydr)oxides this behaviour was also observed in earlier work for various organic acid anions (Hinsinger 2001; Jones and Brassington 1998). Generally, organic acid anions with one or more carboxylate groups are thought to behave in similar manners as P when it comes to sorption to Fe- and Al-(hydr)oxides since they also have O<sup>2-</sup> ligands adsorbing to the surface and are thus as affected as P to changes in surface charge. Sorption has been observed to often correlate with the amount of carboxylate groups of the acid. The more charge the acid anion has, the higher the sorption. For goethite, citrate with three carboxylate groups (charge of -3) had the highest sorption, followed by Ox (-2) and lactate (-1) (Filius et al. 1997). In the case of Fh, Ox exhibited the strongest sorption behaviour before citrate, malonate (-2) and acetate (-1) which was the weakest (Jones and Brassington 1998).

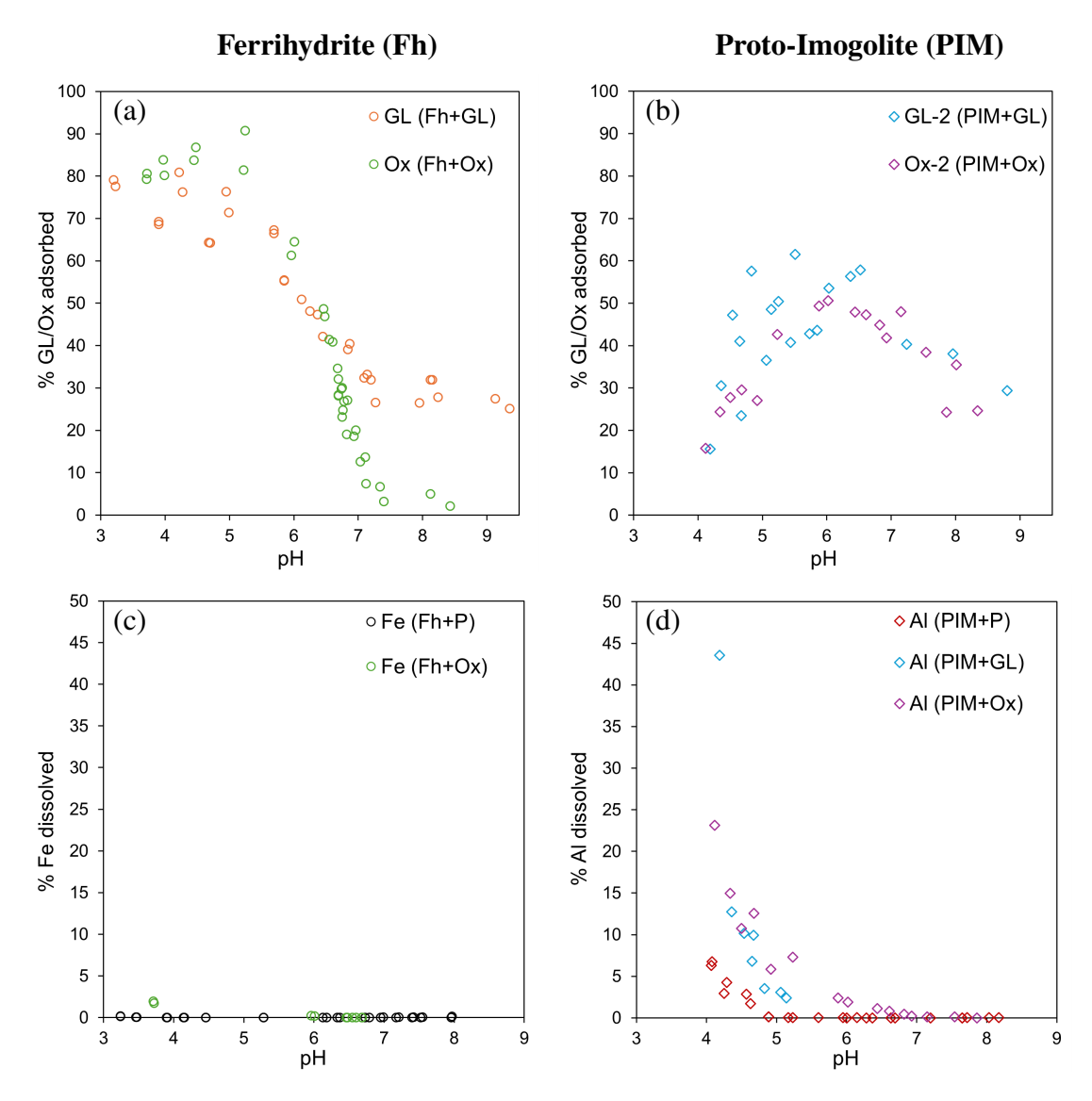


**Figure 9:** Acid anion sorption to a) Fh and b) PIM as a function of pH in the single sorbent systems; c) dissolved Fe and d) dissolved Al in the single sorbent systems. For data of the competitive systems see Figure 10 and Figure 11. Systems with Fh are presented as circles, systems with PIM as diamonds. GL-2 and Ox-2 refer to data points of only the second replicate (see section 5.1.5).

Contrary to this, in this thesis Ox and GL were found to have similar amount of sorption when looking at either Fh or PIM throughout most of the studied pH range. Here, the clear difference lies between the minerals (Figure 9a,b).

#### **Acid Anion Sorption to Ferrihydrite**

At low pH around 80% of GL and Ox are sorbed to Fh with Ox being sorbed slightly more strongly. It should be noted though, that the DOC measurement of the input GL solution gave  $27.3 \,\mathrm{mgL^{-1}}$ , amounting to  $0.38 \,\mathrm{mM}$  compared to  $0.40 \,\mathrm{mM}$  for Ox. At very low pH values that are below the p $K_a$  value of the acid (Table 1), the acid anion becomes increasingly protonated, leading to the maximum adsorption value and a plateau. Some data points show sorption up to 90% at pH 5.2 for Ox, although the replicate at the same pH is only 81%. In contrast, GL shows data points as low as 64% (pH 4.7), but also up to 81% (pH 4.2) at low pH values. From

pH 4.6, GL sorption slowly decreases until reaching a plateau of 26–32% at pH 7.3. Sorption of Ox starts decreasing at higher pH values between 5.2 and 6.4, but more rapidly. At pH 6.6 GL and Ox are sorbed in equal strength (41%). Ox continues to decrease steeply as the pH slowly rises, with almost all Ox being free in solution at pH 7.4 (only 3% sorbed). As will be discussed later in the modelling section, best results were obtained when assuming that Ox binds as bidentate inner-sphere complexes at edge-sharing sites, while GL was only bound as outer-sphere complexes via hydrogen bonding. The author suspects that this explains the small difference in the sorption behaviour of Ox and GL to Fh. Outer-sphere complexes are more weakly bound, thus more easily released, when the pH increases. Inner-sphere complexes bind directly to the surface. As the pH increases, surface groups without Ox are likely to be neutralised first. As the pH approaches the PZC, no more  $\equiv$ FeOH<sub>2</sub><sup>1/2+</sup> surface groups are present that could be exchanged for the carboxylate ligands from Ox, leading to 0% Ox sorption. Opposite to this, hydrogen bonding can still occur between a positively polarised H of the ≡FeOH<sup>1/2−</sup> surface ligand and a negatively charged O of the carboxylate group of GL, or the negatively polarised O of the OH group of GL or between the negatively charged O of the  $\equiv$ FeOH<sup>1/2-</sup> surface ligand and the H of the OH group.

In addition, Ox is able to dissolve Fh, although only to small extent. The highest amount of dissolved Fe is 1.7% at pH 3.7. The Fe content of the system Fh+GL was not measured (Figure 9c), however, it is assumed that GL is hardly able to dissolve Fh based on the dissolved Fe in the competitive system Fh+P+GL (Figure 10c). This will be discussed in section 5.1.3.

#### **Acid Anion Sorption to Proto-Imogolite**

Contrary to Fh, the maximum amount of acid anion sorption (between 40% and 60%) to PIM lies between pH 5.5 and 6.5 (Figure 9b). Towards more acidic and more alkaline pH, the sorption decreases for both GL and Ox. It is difficult to say whether the affinity is higher for GL or Ox, since there are GL data points at similar pH values higher and lower than Ox. As will be explained later (section 5.1.5), the filters used released organic carbon (OC), which means that the values of the data points are not entirely precise. Nevertheless, GL and Ox sorption to PIM follows a similar trend at comparable values. The sorption behaviour is explained the same way as for P, by a decrease in positively charged sorption sites towards higher pH, resulting in less sorption and by the dissolution of PIM towards lower pH. In comparison to Fh, both GL and Ox do not reach 0% sorption at high pH within the measured pH range. This is attributed to the high PZC of around 10-11 for the ≡AlOH surface groups (Gustafsson 2001b). Both anions increase the amount of dissolved PIM by up to three times compared to the system of PIM+P without additional acid (Figure 9d). The mechanism behind this ligand-promoted dissolution is predominantly due to ligand adsorption and the dissociation of the Metal(III)ligand complexes from the surface. A low pH favours this process due to the protonation of OH groups on the oxide surface. This weakens the Al-O bonds and allows H<sub>2</sub>O ligands to be released more easily than OH ligands, or allows for greater sorption due to more positive charge on the surface (Cornell and Schwertmann 2003). The lower the pH value, the greater the proportion of PIM dissolved in the solution. At pH 4.2 44% Al is dissolved in the PIM+GL system, while at a pH of 4.1 for PIM+Ox it is 23%. At pH 6.7 it is 10% for PIM+GL and 13% for PIM+Ox, giving a steeper decrease for GL, which reaches 0% dissolution at lower pH (2.4% dissolved Al at pH 5.1), compared to Ox, which still dissolves 2.4% at the pH 5.9.

This confirms the hypothesis that PIM, due to its lower thermodynamic stability, is dissolved

more readily by organic acids than Fh. Even if one takes into account that PIM generally tends to dissolve at low pH, the absolute values for dissolved Al in the single sorbent systems with the acid anions are significantly higher than for Fh (Figure 9c,d, 10c,d).

#### 5.1.3 Sorption in the Competitive Systems

As expected, in all systems with two anions, competition for binding sites was observed. More ligands are present for the same number of sorption sites, resulting in less P, GL and Ox sorption as compared to the single sorbent systems (Figure 10a,b, 11). However, the effectiveness of the acid anions in mobilising P is different for both minerals and both acids studied, as well as the mechanism behind it.

#### **Competitive Sorption to Ferrihydrite**

Dissolved Fe (Figure 10c) shows that Ox is able to dissolve little Fh in the competitive systems at low pH values. The highest measured value for Fh+P+Ox is 3.9% at a pH of 3.9, while dissolved Fe for Fh+P+GL stays 0% indicating that GL is not able to dissolve Fh at all in the competitive system. Previous work has shown that Ox has an even stronger dissolution behaviour on Fh, about 18% at pH 4.0 in a system together with P (Johnson and Loeppert 2006). This is probably due to higher proportional loadings of Ox and P relative to Fh that they used in the study.

Ox sorption to Fh is up to 10% higher than GL sorption in the competitive systems throughout the whole studied pH range. Together with Ox dissolving some Fh at low pH values until pH 6, Ox should reduce P sorption more than GL. However, P is sorbed to the same extent at low pH values in both systems Fh+P+GL and Fh+P+Ox. At pH values above 6, P sorption is even higher for Fh+P+Ox and not Fh+P+GL. This is thought to be due to a difference in SSA of Fh. This results either from different syntheses and storage times of Fh (explained in section 5.1.4) or from Ox being better at preventing or reversing aggregation of Fh, leading to a higher SSA, thus more binding sites that are available for P sorption.

#### **Competitive Sorption to Proto-Imagalite**

The most significant difference in P sorption between single sorbent and competitive systems can be seen for the system PIM+P+Ox, in which at a pH of 4.9 only 81% P was sorbed compared to 99% P sorption in the PIM+P system. Ox significantly reduces the sorption of P on PIM in contrast to GL in the pH range of 4.1 to 6.4. This is thought to be due to the interaction of two different mechanisms. First, in the competitive system nearly 10% more Ox than GL is sorbed between pH 5 and 6.6, occupying more sorption sites, that P can then not bind to. Secondly, Ox promotes dissolution of PIM, even though dissolved Al shows that P inhibits the capacity of the acid anions to dissolve PIM, especially at low pH until pH 5.2. Dissolved Al is 5-10% lower in the competitive systems as compared to the single sorbent systems. While GL was able to mobilise some Al in the single sorbent system, within the competitive system, the amount of dissolved Al is the same as to PIM+P, suggesting that GL does not dissolve any more PIM as PIM is dissolved either way due to the low pH. In contrast, Ox is still able to dissolve about 4-5% more PIM within the competitive system compared to PIM+P.

At higher pH above 6.6, sorption of P is the same in both systems, PIM+P+GL and PIM+P+Ox. Above pH 6.9, Al dissolution in PIM+P+Ox approaches 0% and the amount of Ox and GL sorption seem to become similar, even though this observation must be taken with caution, since it only

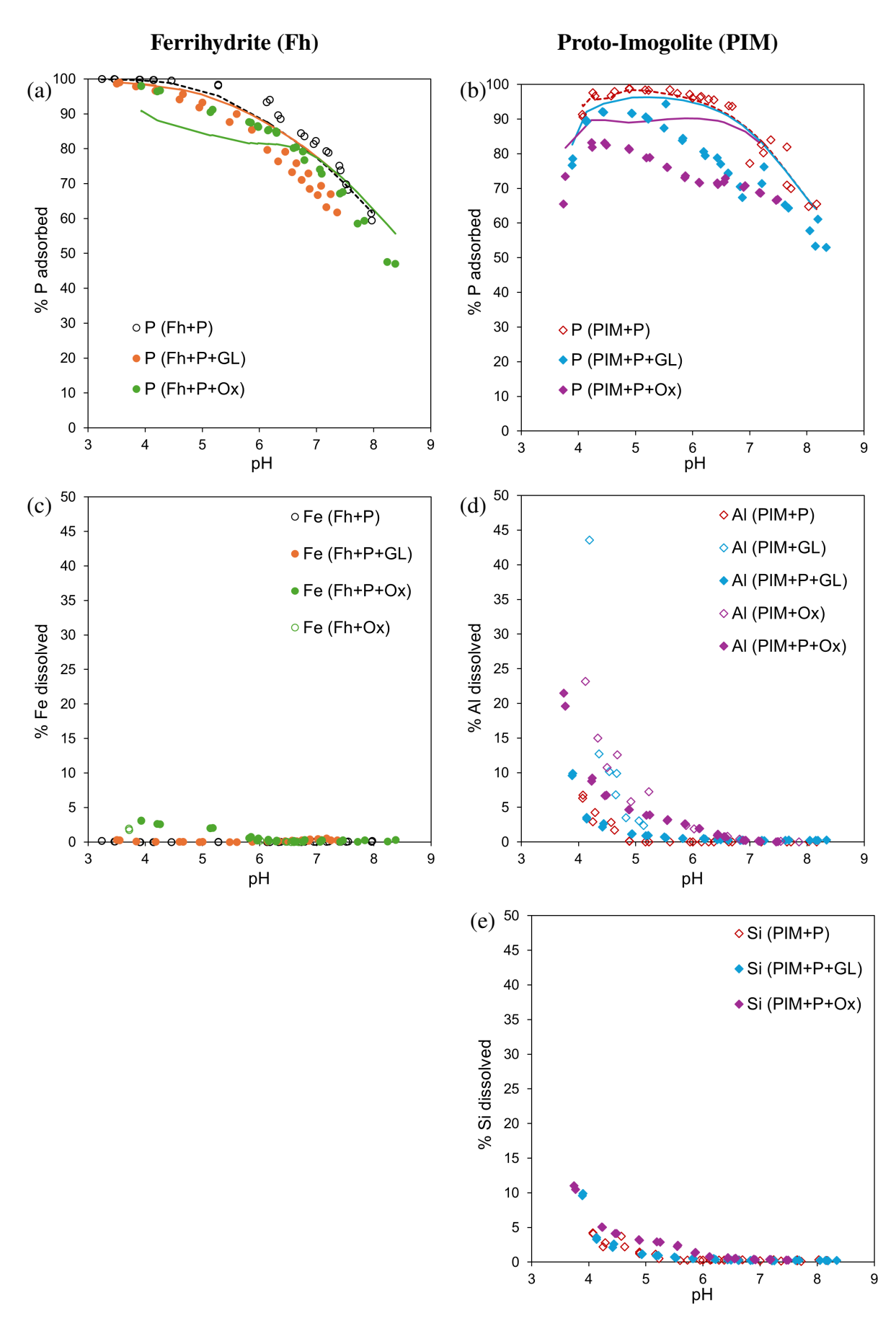


**Figure 10:** Sorption/Dissolution behaviour as a function of pH for Fh (left, circle) and PIM (right, diamond): Amount of a) P sorbed to Fh, b) P sorbed to PIM, c) dissolved Fe, d) dissolved Al, e) dissolved Si. Full symbols represent a competitive system, while empty symbols represent the individual systems. Lines are the modelling results from Visual MINTEQ.

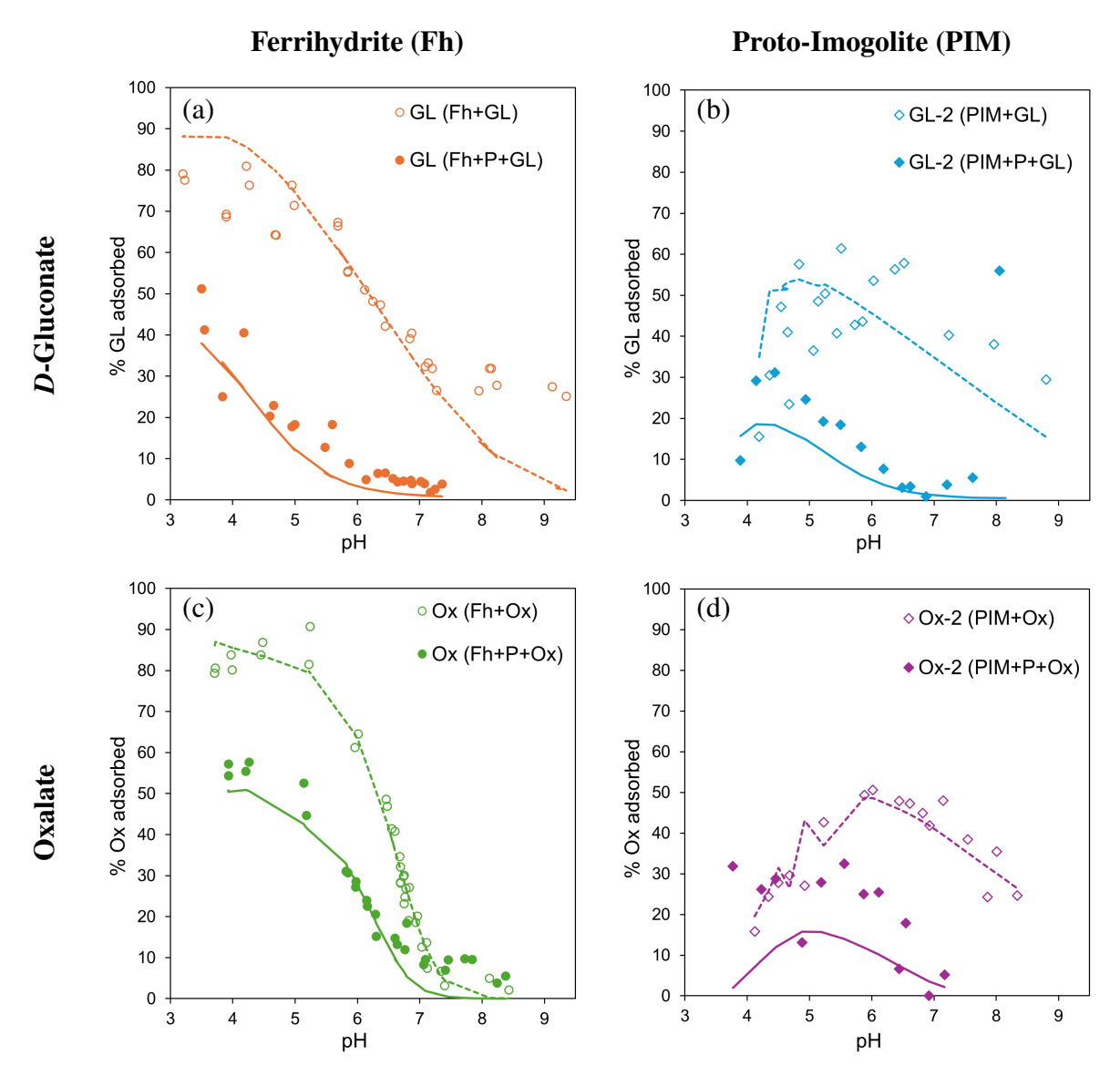


**Figure 11:** Sorption behaviour as a function of pH of a, b) *D*-gluconate and c, d) oxalate for Fh and PIM as both single sorbent (empty symbol) and competitive system with P (full symbol). Systems with Fh are presented as circles, systems with PIM as diamonds. Lines are the modelling results from Visual MINTEQ (dotted line for individual system, full line for competitive system). GL-2 and Ox-2 refer to data points of only the second replicate (see section 5.1.5).

refers to two data points from PIM+P+Ox and, as shortly mentioned, contamination through filters probably does not give exact absolute values (more detailed in section 5.1.5). Nevertheless, this would explain why also P sorption becomes the same in both systems (PIM+P+GL, PIM+P+Ox). They also approach similar values as found for P sorption in PIM+P, although the GL and Ox sorption is increasing again from pH 6.9 towards higher pH. It seems that at pH values above 6.9, the acid anions do not influence the P sorption behaviour anymore. They could possibly bind to negatively charged surface groups through hydrogen bonding and thus not compete with P for the remaining positively charged surface groups.

#### **Comparison and Summary**

Both acid anions were able to mobilise more P from PIM than from Fh. Below the pH of 4.9 significantly more P is free in solution for all PIM systems compared to the Fh systems due to the dissolution behaviour of PIM at low pH values. While both acid anions have the similar ability to inhibit P sorption to Fh, Ox releases up to double the amount of P from PIM in comparison with GL, since Ox allows for even more PIM dissolution. Above a pH of 4.9, P sorption was similarly strong in the systems of Fh+P+GL (pH 5.0: 93% P sorbed), Fh+P+Ox (pH 5.1: 90% P sorbed) and PIM+P+GL (pH 4.9: 92% P sorbed) decreasing towards higher pH. Since in the single sorbent system of PIM+P, P was originally more strongly sorbed to PIM compared to Fh, it suggests that GL is better at mobilising P from PIM than from Fh. This especially applies at pH values higher than 6.3, when the difference in P sorption between Fh (84% P adsorption) and PIM (96% P adsorption) in single sorbent systems becomes greater.

Ox inhibits P sorption to Fh and PIM mostly through its ability of ligand-promoted dissolution, while GL does not allow for any mineral dissolution in the competitive systems. GL inhibits P sorption only by competition. The dissolution behaviour of Ox is more profound for PIM than Fh, suggesting higher affinity for Al(III) than Fe(III) and confirming the hypothesis of a stronger dissolution of PIM together with higher P release.

In the competitive systems, both minerals exhibit stronger affinity for Ox than GL for most of the studied pH range. Nevertheless, above pH 6 for Fh and above 6.6 for PIM, P sorption becomes similar for both Ox or GL. This is attributed to Ox not being able to favour dissolution anymore and thus competition being the only mechanism for the mobilisation of P present.

### 5.1.4 Storage Time of Fh

Batch experiments with Fh were carried out at different days after the synthesis. The sorption behaviour of P to Fh is weaker for experiments in which Fh was used after several days of storage in the fridge (Figure 12). Using the results in Visual MINTEQ, this could be attributed to a decrease in SSA when Fh was used after a longer storage time. Visual MINTEQ predicts a SSA of 611 m<sup>2</sup>g<sup>-1</sup> when Fh is used directly after back-titration, whereas it is only 420 m<sup>2</sup>g<sup>-1</sup> when it had been synthesised 19 days prior to the batch experiment with P (Figure 12a). Since Fh is thermodynamically unstable, Fh particles will grow over time and form aggregates (Hiemstra et al. 2019), thus decreasing the SSA, which in turn leads to less P sorption. Also, the sorption capacity decreases faster for the 420 m<sup>2</sup>g<sup>-1</sup> SSA with increasing pH as compared to the 611 m<sup>2</sup>g<sup>-1</sup> SSA. The surface of Fh is strongly curved and the particle size determines surface charge density. This can be explained by an increasing curvature of the surface that increases the amount of ions that can approach the surface from all directions (Mendez and Hiemstra 2020; Abbas et al. 2008). Less charge density and less ions being attracted to the surface means that an increase in pH, which reduces the amount of positive charge on the Fh surface, has a relatively greater effect on a smaller SSA than on a higher one. Therefore, batch experiments using Ox and GL need to be handled with care. However, in the series of Fh+P+GL, the amount of sorbed GL and P is very similar between experiments carried out directly after synthesis or after one month storage (Figure 12c,d). This might be attributed to the GL anion reversing some of the aggregation. It has been shown before that acid anions can slow the Fh crystallisation down (Jambor and Dutrizac 1998). In addition, Ox has been demonstrated to be capable of disintegrating aggregates (Li et al. 2018). Another plausible explanation is a difference in SSA of Fh directly after the synthesis. The results of the Fh+P+GL here are from two different Fh syntheses. Small differences in the conditions

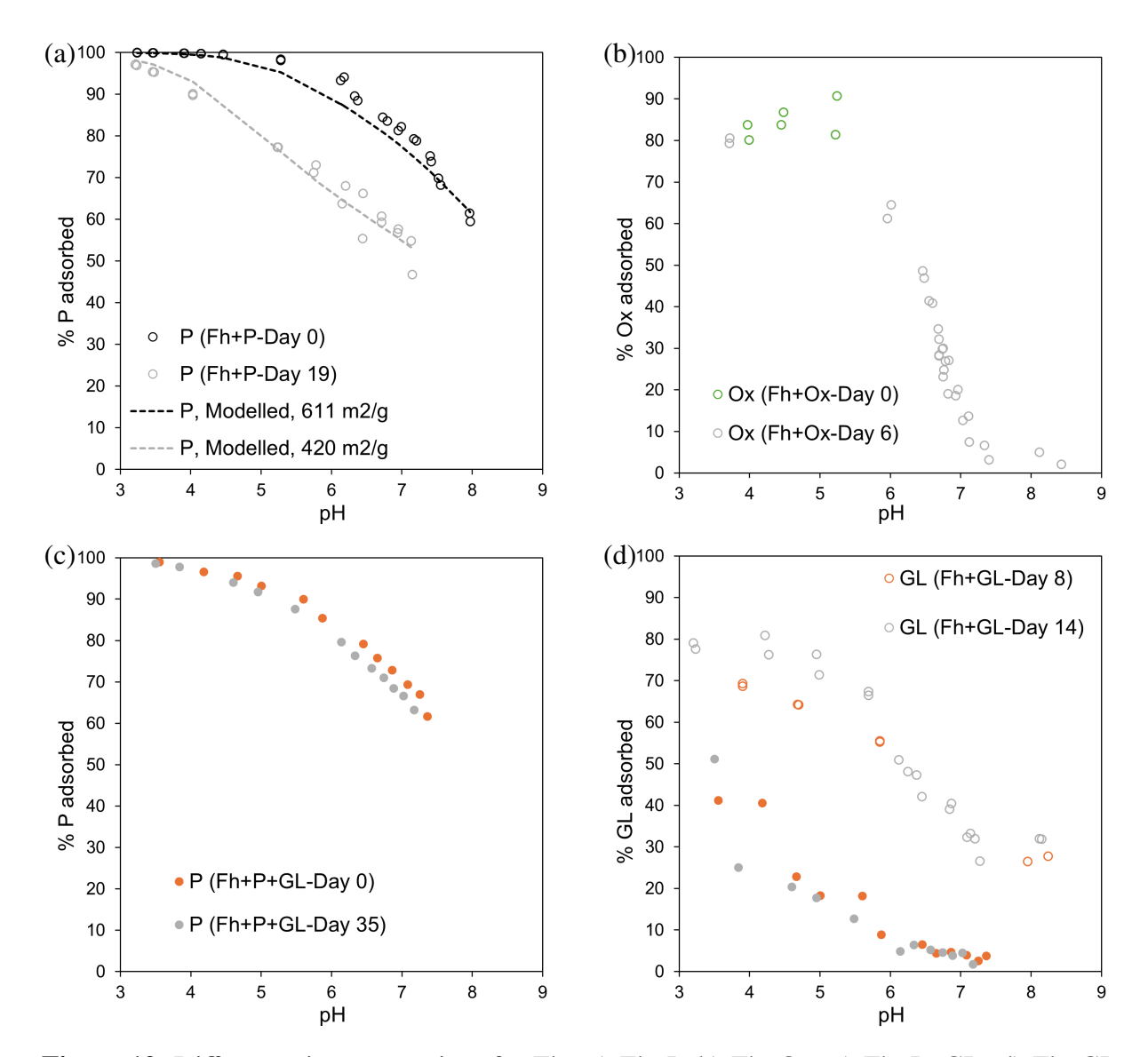


**Figure 12:** Difference in storage time for Fh: a) Fh+P, b) Fh+Ox, c) Fh+P+GL, d) Fh+GL and Fh+P+GL. The longer storage time is shown in grey in each case. Full circles represent a competitive system, while empty circles represent the individual systems.

when preparing Fh can already result in Fh particles of different sizes (Mendez and Hiemstra 2020). Fh+GL was conducted after 6 and 14 days, yielding consistent results in both cases (Figure 12d). Fh+P+Ox was performed 2 and 0 days after synthesis, while Fh+Ox (Figure 12b) was carried out 6 days after synthesis. Within this storage time, the author suspects that the decrease in Fh's SSA will not be substantial, and that the results will correspond well enough to build a credible model. All series are included in this thesis, with the exception of Fh+P-Day 19.

For future reference, all batch experiments should be conducted immediately after the back titration, using the same Fh. However, due to time constraints, and given that the trend is clearly visible, the experiments were not repeated. It is suspected that the results would not differ significantly.

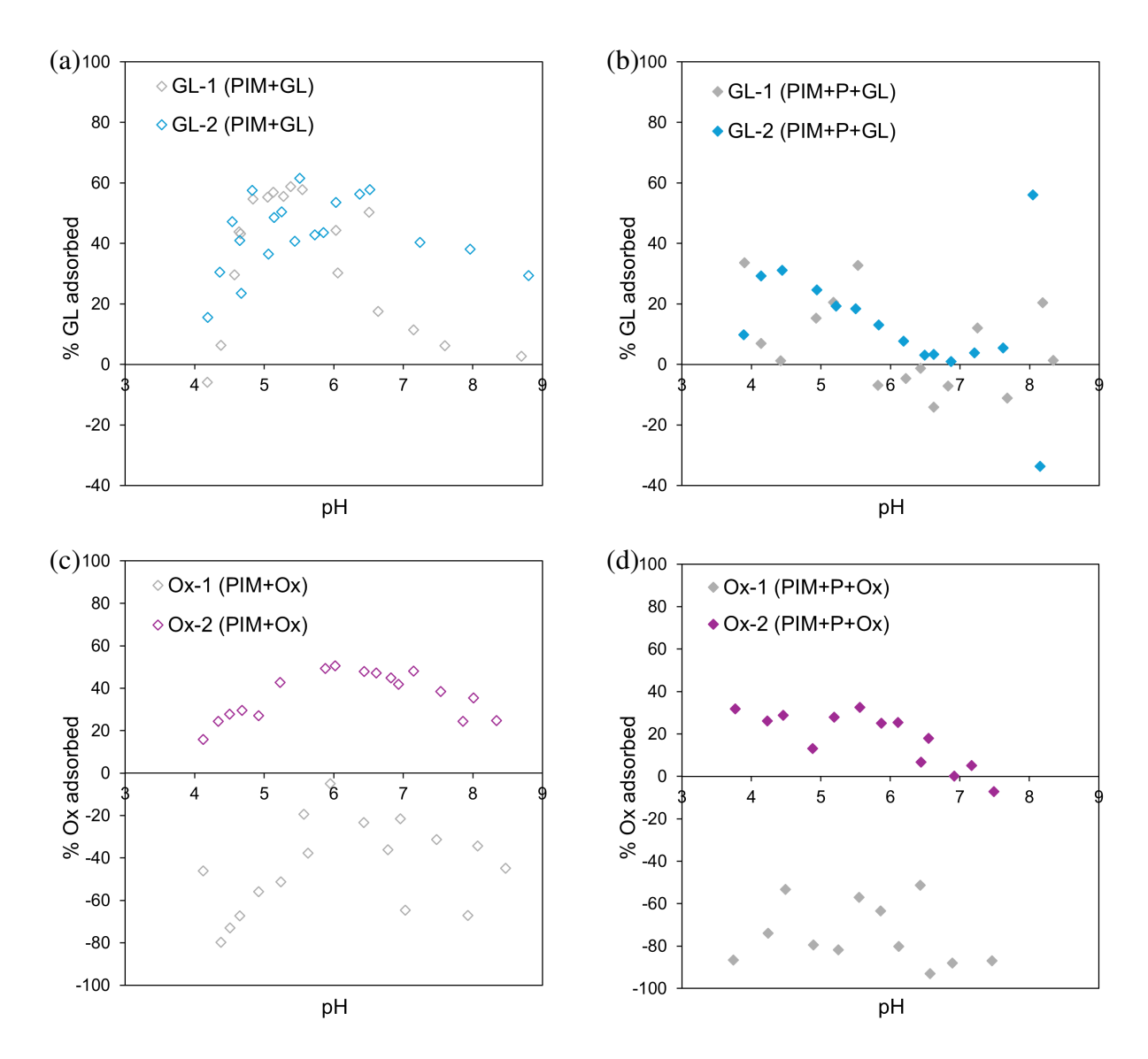


**Figure 13:** OC contamination through the 10 kDa centrifugal devices in the series of a) PIM+GL, b) PIM+P+GL, c) PIM+Ox, d) PIM+P+Ox. The replicate that was not used for further analysis is displayed in grey. Full diamonds represent a competitive system, while empty diamonds represent the individual systems.

## 5.1.5 Contamination through Filters

Unreasonably high amounts of DOC were found in all PIM series containing GL or Ox, exceeding the initial input amount of GL or Ox, resulting in negative sorbed percentage values for GL and Ox (Figure 13). This could be traced back to the 10 kDa centrifugal devices used for filtering after the 19 h equilibration time. Rinsing the filters once with MilliQ water and then analysing new MilliQ water after filtering through the same device resulted in 2.7 mgL<sup>-1</sup> and 3.3 mgL<sup>-1</sup> DOC, suggesting the release of DOC from the 10 kDa centrifugal devices. As some of the DOC results were almost double the input amount, particularly in the PIM+Ox and PIM+P+Ox series, it is highly probable that the acids in the solution are releasing even more DOC from the filters than just MilliQ water alone. It is also very likely that the amount of DOC from the filters differs slightly per sample. Thus, it does not make sense to correct the obtained DOC results by subtracting a predetermined amount.

When comparing the two replicates in each series, it was found that one replicate in each series had significantly lower DOC values, which are within realistic values for the adsorption of organic acid anions. One replicate was filtered through the same centrifugal device as the other replicate, after having been washed with MilliQ water in between. This leads to the assumption that the prevailing DOC in the device was released during the first three centrifugation cycles (namely MilliQ water, first replicate, MilliQ water) and that the DOC then measured in the second replicate is accurate enough to be used for data interpretation and modelling. Therefore, when considering the GL and Ox sorption data, only the replicate that was filtered second is considered, while all data points for P adsorption and Al and Si dissolution are used. Nevertheless, it should be noted that the DOC values used may not be completely accurate. For future work that involves the usage of 10 kDa centrifugal devices from Pall Corporation, Ann Arbor, MI, USA, they should be rinsed (centrifuged) three times with diluted HNO<sub>3</sub> and one time with MilliQ water prior to use to prevent any OC contamination, as was done in earlier work by Löv et al. (2017) (0.001 M HNO<sub>3</sub>).

## 5.2 Modelling Results

### 5.2.1 Modelling Ferrihydrite

Modelling of P sorption to Fh has previously been optimised by Gustafsson and Antelo (2022). Using the same conditions and parameters – that is, having bidentate complexes only on cornersharing sites, resulting in five surface complexes (see Table 2) – experimental observations could be simulated well (Figure 10a). The small underestimation of the model of around 5% from pH values higher than 5.3 is probably due to the difference in temperature. Surface complexation constants were reported for 22°C, while batch experiments in this thesis were carried out at 8°C. Nevertheless, this small difference is thought to be reasonable and was not further treated by optimising constants for 8°C.

For Ox sorption, best results were obtained by assuming that Ox binds as inner-sphere binuclear bidentate complex only at edge sharing sites (Figure 11c). ATR-FTIR data showed that Ox could be present as four different species depending on the Ox/Fe ratio and the aggregation state of Fh. Li et al. (2018) found binuclear bidentate complexes to dominate at Ox/Fe ratios of 0.01-0.1, gradually shifting to mononuclear bidentate complexes dominating at Ox/Fe ratios of 0.2-0.5. Furthermore, some outer-sphere complexes were detected at Ox/Fe ratios of 0.1-0.5 and aqueous Ox species. They suggest that the binuclear bidentate complexes are the reason for colloidal particles being released from larger Fh aggregates due to electrostatic repulsion which leads to an increase in surface area and more Ox being sorbed as mononuclear bidentate complexes, which leads to enhanced dissolution of Fh. Low molecular weight anions sorbed as mononuclear bidentate complexes typically promote mineral dissolution while those in a binuclear bidentate mode inhibit it, because of the high activation energy that needs to be overcome when the ligand has to dissociate from two metal cations at once (Johnson et al. 2005). This explains the observed difference in the amount of Fe dissolution to the findings of Johnson and Loeppert (2006). The Ox/Fe ratio in this thesis is 1.3, suggesting that most Ox will be sorbed as binuclear bidentate complex, as also well predicted by the model, inhibiting Fh dissolution. There might also be some mononuclear bidentate complexes present that are responsible for the little observed dissolved Fe. However, the inclusion of such complexes did not lead to better modelling and was therefore not taken into account. Using the optimised constants for the sorption of Ox to Fh, the modelling results for the competing sorption of P and Ox to Fh were acceptable.

At low and high pH values, Ox sorption was slightly underestimated (Figure 11c). However, experimental results between pH 5.8 and 6.5 were accurately presented. Experimentally, P sorption decreased more linearly with increasing pH, whereas modelling underestimated P sorption at low pH and overestimated it at pH above 6.8, resulting in a flat S-shaped curve (Figure 10a).

GL sorption to Fh was also well predicted for most of the pH range when GL was allowed to bind as outer-sphere complexes for all edge- and corner-sharing single coordinated, as well as triply coordinated sites (Figure 11a). Other mono-carboxylates, such as acetate, benzoate and cyclohexanecarboxylate were also found to bind as two different types of outer-sphere complexes to the goethite surface. In one case, the carboxylate group directly shared hydrogen bonds with the  $H_2O$  or OH groups on the surface of goethite. In the other, a  $H_2O$  molecule separates the surface from the carboxylate ligand (Norén and Persson 2007). Therefore, they suggested that surface complexation modelling should consider both types of outer-sphere complexes. Even though all three mono-carboxylates approached 0 sorption to goethite at higher pH in contrast to the found  $25{\text -}30\%$  sorption of GL to Fh in this thesis, the author suspects that not taking into account different types of outer-sphere complexes could be the reason for the presented model to underestimate GL sorption at high pH, as well as the slight overestimation at low pH. In the competitive system of Fh+P+GL, the optimised model parameters constantly slightly underestimate GL sorption (Figure 11a) as well as overestimate P sorption (Figure 10a) with bigger difference to the experimental results at higher pH values in the case of P sorption.

#### 5.2.2 Modelling Proto-Imogolite

Adsorption to PIM was modelled with the Basic Stern Model from Florén et al. (in preparation) with the only reactive surface site being  $\equiv$ AlOH.  $PO_4^{3-}$  and  $HPO_4^{2-}$  were allowed to bind as binuclear bidentate complexes and  $H_2PO_4^{-}$  was not included (Table 3). Using similar CD values as for Fh yielded optimised log K values that were able to successfully describe the P sorption to PIM in the studied pH range (Figure 10b).

Assuming that Ox binds to PIM as an outer-sphere mononuclear monodentate complex represented Ox sorption behaviour the best (Figure 11d). However, best fit only gave an *R* value of 0.865. The model gives two lower points at pH 4.7 and pH 5.2 instead of following a continuous trend that cannot be explained. This will probably lead to a lower correlation between experimental and modelled values, and there is also the uncertainty factor that the absolute experimental values are correct. Within the competitive system, Ox sorption is clearly underestimated (Figure 11d), while P sorption is overestimated, giving a local minimum at pH 4.9 and a local maximum at pH 6.6, while in the experimental data the curve shows maximum adsorption at pH 4.2 and has local minimum at pH 6.2 (Figure 10b).

The best results for GL sorption to PIM (Figure 11b) as outer-sphere complexes were achieved with an *R* value of only 0.322. Since experimental data can show differences of up to 18% in GL sorption at a similar measured pH value, it is difficult to use them as input for calibrating the model. It is hard to define absolute values, even though a trend is clearly visible. In spite of the poor *R* value for GL sorption in the single sorbent system, the model for GL sorption in the competitive system is more reliable (Figure 11b). The modelled curve is flatter compared to the experimental one underestimating GL sorption at a pH of 4.4 by 13% and towards a pH of 6.2 by only 4%. However, it could not model the P sorption accurately, giving nearly the same curve as for the single sorbent system PIM+P without acid, overestimating the P sorption in the

competitive system (Figure 10b).

Those findings question if there might be other P surface complexes additionally to the ones used in the modelling, even though they seemed to resemble the P sorption in the single sorbent system of PIM+P pretty precisely. Furthermore, due to filter contamination, acid anion adsorption values are not absolute and would give somewhat different log K values which would in turn affect the sorption in the competitive system. Another reason for the difference in modelling and experimental data is the model used that is still under progress. Some of the fundamental properties, such as the SSA, the site density and the inner capacitance might need adjustment. More detailed information on surface-charge properties of PIM would be useful in order to improve input parameters.

## 6 Conclusion

P sorption and the influence of two organic acid anions GL and Ox on the two common minerals in Swedish forest soils Fh and PIM, as representative of ITN, was investigated. This behaviour was later modelled in Visual MINTEQ.

Generally, P sorption to both minerals was high, ranging from 60% to nearly 100% throughout the studied pH range. P, GL and Ox sorption decreased with increasing pH due to the reduction in positively charged surface groups available for binding. Both minerals had higher affinity for P than for Ox and GL. Furthermore, P exhibited higher affinity for PIM than for Fh above pH 5.5 attributed to the higher SSA of PIM, as well as the formation of amorphous Al-P precipitates and the higher intrinsic adsorption constants of Al-(hydr)oxides compared to Fe-(hydr)oxides. At pH values below 4.9 PIM dissolved, decreasing the available number of sorption sites leading to decreasing P sorption, while P sorption was nearly 100% for Fh.

In the single sorbent systems, the amount of GL and Ox sorption was similar for the same mineral. Ox was slightly more strongly sorbed to Fh at low pH, with the sorption decreasing steeper and becoming lower towards high pH compared to GL. This small difference was explained by the different binding behaviours of the anions, with Ox being bound as more stable inner-sphere binculear bidentate complexes and GL as outer-sphere complexes via hydrogen bonding. This was supported by modelling results. Additionally, Ox was able to dissolve little Fh at low pH, while GL did not show any dissolution ability at all.

As hypothesised, this dissolution ability was more profound for PIM. Here, both acid anions were able to dissolve PIM at low pH. However, in the competitive systems P was found to reduce mineral dissolution by Ox and completely inhibit it for GL.

In the competitive systems both GL and Ox reduced P sorption, but to different extents depending on the mineral and the acid anion. Ox's ability to significantly dissolve PIM was found to be the major reason for the greater reduction in P sorption in PIM+P+Ox compared to PIM+P+GL, Fh+P+GL and Fh+P+Ox. When Ox does not promote dissolution anymore above pH 6 for Fh and 6.6 for PIM, P sorption actually becomes similar for both Ox and GL and is even higher in the Fh+P+Ox system than in the Fh+P+GL system.

The Fh-CD-MUSIC model by Gustafsson and Antelo (2022) successfully described P sorption to Fh, and the optimisation of the constants for Ox and GL sorption simulated their behaviour well, but could not accurately represent P sorption in competitive systems, reflecting the complexity of such systems and the need for further investigation. P sorption to PIM could also be accurately predicted using Florén's Basic Stern Model (in preparation), but not in the competitive systems with organic acid anions. Contamination of the samples by the filters led to inaccurate DOC levels for both GL and Ox, making it more difficult to obtain satisfactory models. Furthermore, these results also show that the basic parameters of the model may need to be adjusted in order to yield values that better fit the observed data.

Overall, in Swedish forest soils, where PIM dominates, these findings contribute to our understanding of P sorption. Particularly at pH values between 4 and 6.5, which are typical for podzolic soils, both GL and Ox were able to release P from Fh and PIM, with a larger proportion

coming from PIM. This suggests that local secretion of LMWOA contributes to making P more bioavailable, which may reduce fertiliser requirements in managed forest soils. Nevertheless, it should be noted that the results do not reflect actual compositions of soil and other interactions might influence the behaviour. While P generally bound more strongly to PIM than to Fh, this only occurred above pH 5.5. The higher proportion of P to Al-(hydr)oxides found also in soils with lower pH values may partly reflect the predominance of PIM or different SSAs of Fh and PIM in soil compared to the synthesised minerals, but may also reflect P's preference for binding to PIM rather than Fh when both minerals are present. Therefore, the next step could involve testing a system with both minerals to study their interactions.

## **Bibliography**

- Abbas, Z., Labbez, C., Nordholm, S., and Ahlberg, E. (2008). "Size-Dependent Surface Charging of Nanoparticles". *The Journal of Physical Chemistry C*, 112(15). DOI: 10.1021/jp709667u
- Adams, F., Bauer, M., Levard, C., and Marc Michel, F. (2024). "Multivariate Regression Analysis of Factors Regulating the Formation of Synthetic Aluminosilicate Nanoparticles". *Nanoscale*, 16(13). DOI: 10.1039/D4NR00473F
- Akselsson, C., Westling, O., Alveteg, M., Thelin, G., Fransson, A.-M., and Hellsten, S. (2008). "The Influence of N Load and Harvest Intensity on the Risk of P Limitation in Swedish Forest Soils". *Science of The Total Environment*, 404(2). DOI: 10.1016/j.scitotenv.2007.11.017
- Almeida, J. P. (2019). "Biomass, Community Structure and Phosphorus Uptake of Ectomycorrhizal Fungi in Response to Phosphorus Limitation and Nitrogen Deposition". Doctoral Thesis. Lund University.
- Amadou, I., Faucon, M.-P., and Houben, D. (2022). "Role of Soil Minerals on Organic Phosphorus Availability and Phosphorus Uptake by Plants". *Geoderma*, 428. DOI: 10.1016/j.geoderma. 2022.116125
- Andersson, M., Carlsson, M., Ladenberger, A., Morris, G., Sadeghi, M., Uhlbäck, J., et al. (2014). "Geochemical Atlas of Sweden". *Geological Survey of Sweden: Uppsala, Sweden*,
- Andrino, A., Boy, J., Mikutta, R., Sauheitl, L., and Guggenberger, G. (2019). "Carbon Investment Required for the Mobilization of Inorganic and Organic Phosphorus Bound to Goethite by an Arbuscular Mycorrhiza (Solanum Lycopersicum x Rhizophagus Irregularis)". *Frontiers in Environmental Science*, 7. DOI: 10.3389/fenvs.2019.00026
- Arai, Y., Elzinga, E. J., and Sparks, D. L. (2001). "X-Ray Absorption Spectroscopic Investigation of Arsenite and Arsenate Adsorption at the Aluminum Oxide—Water Interface". *Journal of Colloid and Interface Science*, 235(1). DOI: 10.1006/jcis.2000.7249
- Arai, Y. and Sparks, D. L. (2001). "ATR-FTIR Spectroscopic Investigation on Phosphate Adsorption Mechanisms at the Ferrihydrite-Water Interface". *Journal of Colloid and Interface Science*, 241(2). DOI: 10.1006/jcis.2001.7773
- Balland, C., Poszwa, A., Leyval, C., and Mustin, C. (2010). "Dissolution Rates of Phyllosilicates as a Function of Bacterial Metabolic Diversity". *Geochimica et Cosmochimica Acta*, 74(19). DOI: 10.1016/j.gca.2010.06.022
- Bethke, C. and Yeakel, S. (2009). "Geochemist's Workbench: Release 8.0 Reaction Modeling Guide: RockWare Incorporated".
- Bhatti, J. S., Comerford, N. B., and Johnston, C. T. (1998). "Influence of Oxalate and Soil Organic Matter on Sorption and Desorption of Phosphate onto a Spodic Horizon". *Soil Science Society of America Journal*, 62(4). DOI: 10.2136/sssaj1998.03615995006200040033x
- Binkley, D. and Högberg, P. (2016). "Tamm Review: Revisiting the Influence of Nitrogen Deposition on Swedish Forests". *Forest Ecology and Management*, 368. DOI: 10.1016/j.foreco.2016.02.035
- Boily, J.-F. and Song, X. (2020). "Direct Identification of Reaction Sites on Ferrihydrite". *Communications Chemistry*, 3(1). DOI: 10.1038/s42004-020-0325-y
- Bundschuh, J. and Zilberbrand, M., eds. (2011). Geochemical Modeling of Groundwater, Vadose and Geothermal Systems. London: CRC Press. DOI: 10.1201/b11690.
- Cismasu, A. C., Michel, F. M., Tcaciuc, A. P., Tyliszczak, T., and Gordon E. Brown, J. (2011). "Composition and structural aspects of naturally occurring ferrihydrite". *Comptes Rendus. Géoscience*, 343(2-3). DOI: 10.1016/j.crte.2010.11.001

- Cornell, R. and Schwertmann, U. (2003). The Iron Oxides: Structure, Properties, Reactions, Occurrences and Uses. 2nd ed. Wiley Online Library. Wiley.
- Courty, P.-E., Buée, M., Diedhiou, A. G., Frey-Klett, P., Le Tacon, F., Rineau, F., Turpault, M.-P., Uroz, S., and Garbaye, J. (2010). "The Role of Ectomycorrhizal Communities in Forest Ecosystem Processes: New Perspectives and Emerging Concepts". *Soil Biology and Biochemistry*, 42(5). DOI: 10.1016/j.soilbio.2009.12.006
- D'Amico, M., Almeida, J. P., Barbieri, S., Castelli, F., Sgura, E., Sineo, G., Martin, M., Bonifacio, E., Wallander, H., and Celi, L. (2020). "Ectomycorrhizal Utilization of Different Phosphorus Sources in a Glacier Forefront in the Italian Alps". *Plant and Soil*, 446(1). DOI: 10.1007/s11104-019-04342-0
- Davis, J. A. and Leckie, J. O. (1978). "Surface Ionization and Complexation at the Oxide/Water Interface II. Surface Properties of Amorphous Iron Oxyhydroxide and Adsorption of Metal Ions". *Journal of Colloid and Interface Science*, 67(1). DOI: 10.1016/0021-9797(78)90217-5
- Dixon, J. B. and Schulze, D. G. (2002). Soil Mineralogy with Environmental Applications.
- Doherty, J. (2010). PEST, Model-Independent Parameter Estimation, User Manual, 5th Ed.; Watermark Numerical Computing.
- Doydora, S., Gatiboni, L., Grieger, K., Hesterberg, D., Jones, J. L., McLamore, E. S., Peters, R., Sozzani, R., Van den Broeck, L., and Duckworth, O. W. (2020). "Accessing Legacy Phosphorus in Soils". *Soil Systems*, 4(4). DOI: 10.3390/soilsystems4040074
- ECHA (2025). European Chemicals Agency Chemicals Data Base. https://chem.echa.europa.eu/. Elser, J. J. and Hamilton, A. (2007). "Stoichiometry and the New Biology: The Future Is Now". *PLOS Biology*, 5(7). DOI: 10.1371/journal.pbio.0050181
- Evanko, C. R. and Dzombak, D. A. (1999). "Surface Complexation Modeling of Organic Acid Sorption to Goethite". *Journal of Colloid and Interface Science*, 214(2). DOI: 10.1006/jcis. 1999.6184
- Farmer, V. C., Adams, M. J., Fraser, A. R., and Palmieri, F. (1983). "Synthetic Imogolite: Properties, Synthesis and Possible Applications". *Clay Minerals*, 18(4). DOI: 10.1180/claymin.1983.018.4.11
- Fernandez-Martinez, A. and Michot, L. J. (2016). "Chapter 9 Physicochemical Properties of Imogolite". In: *Developments in Clay Science*. Ed. by Yuan, P., Thill, A., and Bergaya, F. Vol. 7. Nanosized Tubular Clay Minerals. Elsevier, pp. 202–222. DOI: 10.1016/B978-0-08-100293-3.00009-1.
- Filius, J. D., Hiemstra, T., and Van Riemsdijk, W. H. (1997). "Adsorption of Small Weak Organic Acids on Goethite: Modeling of Mechanisms". *Journal of Colloid and Interface Science*, 195(2). DOI: 10.1006/jcis.1997.5152
- Florén, T., Díaz, M. B., Cornelis, G., Hillier, S., and Gustafsson, J. P. (2025). "Characterization of Imogolite-Type Nanoparticles in Podzols: Morphology and Association with Iron". *Geoderma*, 459. DOI: 10.1016/j.geoderma.2025.117376
- Fox, T. R. and Comerford, N. B. (1990). "Low-Molecular-Weight Organic Acids in Selected Forest Soils of the Southeastern USA". *Soil Science Society of America Journal*, 54(4). DOI: 10.2136/sssaj1990.03615995005400040037x
- Goldberg, S. (2002). "Competitive Adsorption of Arsenate and Arsenite on Oxides and Clay Minerals". *Soil Science Society of America Journal*, 66(2). DOI: 10.2136/sssaj2002.4130
- Griffiths, R. P., Baham, J. E., and Caldwell, B. A. (1994). "Soil Solution Chemistry of Ectomy-corrhizal Mats in Forest Soil". *Soil Biology and Biochemistry*, 26(3). DOI: 10.1016/0038-0717(94)90282-8

- Gustafsson, J. P. (2001a). "Modelling Competitive Anion Adsorption on Oxide Minerals and an Allophane-Containing Soil". *European Journal of Soil Science*, 52(4). DOI: 10.1046/j.1365-2389.2001.00414.x
- Gustafsson, J. P., Berggren, D., Simonsson, M., Zysset, M., and Mulder, J. (2001). "Aluminium Solubility Mechanisms in Moderately Acid Bs Horizons of Podzolized Soils". *European Journal of Soil Science*, 52(4). DOI: 10.1046/j.1365-2389.2001.00400.x
- Gustafsson, J., Karltun, E., and Bhattacharya, P. (1998). Allophane and Imogolite in Swedish Soils.
- Gustafsson, J. P. (2001b). "The Surface Chemistry of Imogolite". *Clays and Clay Minerals*, 49(1). DOI: 10.1346/CCMN.2001.0490106
- (2003). "Modelling Molybdate and Tungstate Adsorption to Ferrihydrite". *Chemical Geology*, 200(1). DOI: 10.1016/S0009-2541(03)00161-X
- (2024a). Visual MINTEQ 4.0 User Guide. Uppsala.
- (2024b). Visual MINTEQ, Version 4.0 Beta. Uppsala.
- Gustafsson, J. P. and Antelo, J. (2022). "Competitive Arsenate and Phosphate Adsorption on Ferrihydrite as Described by the CD-MUSIC Model". *ACS Earth and Space Chemistry*, 6(5). DOI: 10.1021/acsearthspacechem.2c00081
- Gustafsson, J. P., Bhattacharya, P., and Karltun, E. (1999). "Mineralogy of Poorly Crystalline Aluminium Phases in the B Horizon of Podzols in Southern Sweden". *Applied Geochemistry*, 14(6). DOI: 10.1016/S0883-2927(99)00002-5
- Hiemstra, T. and Van Riemsdijk, W. H. (1996). "A Surface Structural Approach to Ion Adsorption: The Charge Distribution (CD) Model". *Journal of Colloid and Interface Science*, 179(2). DOI: 10.1006/jcis.1996.0242
- Hiemstra, T. (2013). "Surface and Mineral Structure of Ferrihydrite". *Geochimica et Cosmochimica Acta*, 105. DOI: 10.1016/j.gca.2012.12.002
- (2015). "Formation, Stability, and Solubility of Metal Oxide Nanoparticles: Surface Entropy, Enthalpy, and Free Energy of Ferrihydrite". *Geochimica et Cosmochimica Acta*, 158. DOI: 10.1016/j.gca.2015.02.032
- (2018). "Surface Structure Controlling Nanoparticle Behavior: Magnetism of Ferrihydrite, Magnetite, and Maghemite". *Environmental Science: Nano*, 5(3). DOI: 10.1039/C7EN01060E
- Hiemstra, T., C. Mendez, J., and Li, J. (2019). "Evolution of the Reactive Surface Area of Ferrihydrite: Time, pH, and Temperature Dependency of Growth by Ostwald Ripening". *Environmental Science: Nano*, 6(3). DOI: 10.1039/C8EN01198B
- Hiemstra, T. and Zhao, W. (2016). "Reactivity of Ferrihydrite and Ferritin in Relation to Surface Structure, Size, and Nanoparticle Formation Studied for Phosphate and Arsenate". *Environmental Science: Nano*, 3(6). DOI: 10.1039/C6EN00061D
- Hinsinger, P. (2001). "Bioavailability of Soil Inorganic P in the Rhizosphere as Affected by Root-Induced Chemical Changes: A Review". *Plant and Soil*, 237(2). DOI: 10.1023/A: 1013351617532
- Jambor, J. L. and Dutrizac, J. E. (1998). "Occurrence and Constitution of Natural and Synthetic Ferrihydrite, a Widespread Iron Oxyhydroxide". *Chemical Reviews*, 98(7). DOI: 10.1021/cr970105t
- Jansa, J., Finlay, R., Wallander, H., Smith, F. A., and Smith, S. E. (2011). "Role of Mycorrhizal Symbioses in Phosphorus Cycling". In: *Phosphorus in Action: Biological Processes in Soil Phosphorus Cycling*. Ed. by Bünemann, E., Oberson, A., and Frossard, E. Berlin, Heidelberg: Springer, pp. 137–168. DOI: 10.1007/978-3-642-15271-9\_6.

- Johnson, B. B., Ivanov, A. V., Antzutkin, O. N., and Forsling, W. (2002). "31P Nuclear Magnetic Resonance Study of the Adsorption of Phosphate and Phenyl Phosphates on  $\gamma$ -Al2O3". *Langmuir*, 18(4). DOI: 10.1021/la001537t
- Johnson, S. E. and Loeppert, R. H. (2006). "Role of Organic Acids in Phosphate Mobilization from Iron Oxide". *Soil Science Society of America Journal*, 70(1). DOI: 10.2136/sssaj2005.0012
- Johnson, S. B., Brown, G. E., Healy, T. W., and Scales, P. J. (2005). "Adsorption of Organic Matter at Mineral/Water Interfaces. 6. Effect of Inner-Sphere versus Outer-Sphere Adsorption on Colloidal Stability". *Langmuir*, 21(14). DOI: 10.1021/la047030q
- Jones, D. L. and Brassington, D. S. (1998). "Sorption of Organic Acids in Acid Soils and Its Implications in the Rhizosphere". *European Journal of Soil Science*, 49(3). DOI: 10.1046/j. 1365-2389.1998.4930447.x
- Jones, D. L. (1998). "Organic Acids in the Rhizosphere a Critical Review". *Plant and Soil*, 205(1). DOI: 10.1023/A:1004356007312
- Jones, D. L. and Oburger, E. (2011). "Solubilization of Phosphorus by Soil Microorganisms". In: *Phosphorus in Action: Biological Processes in Soil Phosphorus Cycling*. Ed. by Bünemann, E., Oberson, A., and Frossard, E. Berlin, Heidelberg: Springer, pp. 169–198. DOI: 10.1007/978-3-642-15271-9\_7.
- Jungqvist, G., Oni, S. K., Teutschbein, C., and Futter, M. N. (2014). "Effect of Climate Change on Soil Temperature in Swedish Boreal Forests". *PLOS ONE*, 9(4). DOI: 10.1371/journal.pone.0093957
- Khalidy, R. and Santos, R. M. (2021). "Assessment of Geochemical Modeling Applications and Research Hot Spots—a Year in Review". *Environmental Geochemistry and Health*, 43(9). DOI: 10.1007/s10653-021-00862-w
- Kleja, D. B., Standring, W., Oughton, D., Gustafsson, J.-P., Fifield, K., and Fraser, A. (2005). "Assessment of Isotopically Exchangeable Al in Soil Materials Using 26Al Tracer". *Geochimica et Cosmochimica Acta*, 69(22). DOI: 10.1016/j.gca.2005.06.010
- Klotzbücher, A., Schunck, F., Klotzbücher, T., Kaiser, K., Glaser, B., Spohn, M., Widdig, M., and Mikutta, R. (2020). "Goethite-Bound Phosphorus in an Acidic Subsoil Is Not Available to Beech (Fagus Sylvatica L.)" *Frontiers in Forests and Global Change*, 3. DOI: 10.3389/ffgc.2020.00094
- Landeweert, R., Hoffland, E., Finlay, R. D., Kuyper, T. W., and van Breemen, N. (2001). "Linking Plants to Rocks: Ectomycorrhizal Fungi Mobilize Nutrients from Minerals". *Trends in Ecology & Evolution*, 16(5). DOI: 10.1016/S0169-5347(01)02122-X
- Larsen, S. (1967). "Soil Phosphorus". In: *Advances in Agronomy*. Ed. by Norman, A. G. Vol. 19. Academic Press, pp. 151–210. DOI: 10.1016/S0065-2113(08)60735-X.
- Levard, C. and Basile-Doelsch, I. (2016). "Chapter 3 Geology and Mineralogy of Imogolite-Type Materials". In: *Developments in Clay Science*. Ed. by Yuan, P., Thill, A., and Bergaya, F. Vol. 7. Nanosized Tubular Clay Minerals. Elsevier, pp. 49–65. DOI: 10.1016/B978-0-08-100293-3.00003-0.
- Levard, C., Doelsch, E., Basile-Doelsch, I., Abidin, Z., Miche, H., Masion, A., Rose, J., Borschneck, D., and Bottero, J. .-. (2012). "Structure and Distribution of Allophanes, Imogolite and Proto-Imogolite in Volcanic Soils". *Geoderma*, 183–184. DOI: 10.1016/j.geoderma. 2012.03.015
- Li, F., Koopal, L., and Tan, W. (2018). "Roles of Different Types of Oxalate Surface Complexes in Dissolution Process of Ferrihydrite Aggregates". *Scientific Reports*, 8(1). DOI: 10.1038/s41598-018-20401-5
- Löv, Å., Sjöstedt, C., Larsbo, M., Persson, I., Gustafsson, J. P., Cornelis, G., and Kleja, D. B. (2017). "Solubility and Transport of Cr(III) in a Historically Contaminated Soil Evidence

- of a Rapidly Reacting Dimeric Cr(III) Organic Matter Complex". *Chemosphere*, 189. doi: 10.1016/j.chemosphere.2017.09.088
- Lundström, U. S., van Breemen, N., and Bain, D. (2000a). "The Podzolization Process. A Review". *Geoderma*, 94(2). DOI: 10.1016/S0016-7061(99)00036-1
- Lundström, U. S., van Breemen, N., Bain, D. C., van Hees, P. A. W., Giesler, R., Gustafsson, J. P., Ilvesniemi, H., Karltun, E., Melkerud, P. .-., Olsson, M., Riise, G., Wahlberg, O., Bergelin, A., Bishop, K., Finlay, R., Jongmans, A. G., Magnusson, T., Mannerkoski, H., Nordgren, A., Nyberg, L., Starr, M., and Tau Strand, L. (2000b). "Advances in Understanding the Podzolization Process Resulting from a Multidisciplinary Study of Three Coniferous Forest Soils in the Nordic Countries". *Geoderma*, 94(2). DOI: 10.1016/S0016-7061(99)00077-4
- Mallet, M., Barthélémy, K., Ruby, C., Renard, A., and Naille, S. (2013). "Investigation of Phosphate Adsorption onto Ferrihydrite by X-ray Photoelectron Spectroscopy". *Journal of Colloid and Interface Science*, 407. DOI: 10.1016/j.jcis.2013.06.049
- Manceau, A. (2012). "Comment on "Direct Observation of Tetrahedrally Coordinated Fe(III) in Ferrihydrite". *Environmental Science & Technology*, 46(12). DOI: 10.1021/es3011749
- Mendez, J. C. and Hiemstra, T. (2020). "Surface Area of Ferrihydrite Consistently Related to Primary Surface Charge, Ion Pair Formation, and Specific Ion Adsorption". *Chemical Geology*, 532. DOI: 10.1016/j.chemgeo.2019.119304
- Merlin, A., Rosolem, C. A., and He, Z. (2016). "Non-Labile Phosphorus Acquisition by Brachiaria". *Journal of Plant Nutrition*, 39(9). DOI: 10.1080/01904167.2015.1109117
- Michel, F. M., Barrón, V., Torrent, J., Morales, M. P., Serna, C. J., Boily, J.-F., Liu, Q., Ambrosini, A., Cismasu, A. C., and Brown, G. E. (2010). "Ordered Ferrimagnetic Form of Ferrihydrite Reveals Links among Structure, Composition, and Magnetism". *Proceedings of the National Academy of Sciences of the United States of America*, 107(7). DOI: 10.1073/pnas.0910170107
- Michel, F. M., Ehm, L., Liu, G., Han, W. Q., Antao, S. M., Chupas, P. J., Lee, P. L., Knorr, K., Eulert, H., Kim, J., Grey, C. P., Celestian, A. J., Gillow, J., Schoonen, M. A. A., Strongin, D. R., and Parise, J. B. (2007a). "Similarities in 2- and 6-Line Ferrihydrite Based on Pair Distribution Function Analysis of X-ray Total Scattering". *Chemistry of Materials*, 19(6). DOI: 10.1021/cm062585n
- Michel, F. M., Ehm, L., Antao, S. M., Lee, P. L., Chupas, P. J., Liu, G., Strongin, D. R., Schoonen, M. A. A., Phillips, B. L., and Parise, J. B. (2007b). "The Structure of Ferrihydrite, a Nanocrystalline Material". *Science*, 316(5832). DOI: 10.1126/science.1142525
- Noh, J. S. and Schwarz, J. A. (1989). "Estimation of the Point of Zero Charge of Simple Oxides by Mass Titration". *Journal of Colloid and Interface Science*, 130(1). DOI: 10.1016/0021-9797(89)90086-6
- Norén, K. and Persson, P. (2007). "Adsorption of Monocarboxylates at the Water/Goethite Interface: The Importance of Hydrogen Bonding". *Geochimica et Cosmochimica Acta*, 71(23). DOI: 10.1016/j.gca.2007.04.037
- Nykvist, N. (1963). "Leaching and Decomposition of Water-Soluble Organic Substances from Different Types of Leaf and Needle Litter". *Studia Forestalia Suecica*,
- Ohashi, F., Tomura, S., Akaku, K., Hayashi, S., and Wada, S.-I. (2004). "Characterization of Synthetic Imogolite Nanotubes as Gas Storage". *Journal of Materials Science*, 39(5). DOI: 10.1023/B: JMSC.0000016188.04444.36
- Parfitt, R. L. (1989). "Phosphate Reactions with Natural Allophane, Ferrihydrite and Goethite". *Journal of Soil Science*, 40(2). DOI: 10.1111/j.1365-2389.1989.tb01280.x
- (2009). "Allophane and Imogolite: Role in Soil Biogeochemical Processes". *Clay Minerals*, 44(1). DOI: 10.1180/claymin.2009.044.1.135

- Parkhurst, D. L. and Appelo, C. a. J. (2013). Description of Input and Examples for PHREEQC Version 3: A Computer Program for Speciation, Batch-Reaction, One-Dimensional Transport, and Inverse Geochemical Calculations. Tech. rep. 6-A43. U.S. Geological Survey. DOI: 10.3133/tm6A43.
- Pauling, L. (1929). "The Principles Determining the Structure of Complex Ionic Crystals". Journal of the American Chemical Society, 51(4). DOI: 10.1021/ja01379a006
- Peacock, C. L. and Sherman, D. M. (2004). "Copper(II) Sorption onto Goethite, Hematite and Lepidocrocite: A Surface Complexation Model Based on Ab Initio Molecular Geometries and EXAFS Spectroscopy". *Geochimica et Cosmochimica Acta*, 68. DOI: 10.1016/j.gca.2003.11.030
- Picot, P., Lange, T., Testard, F., Gobeaux, F., and Thill, A. (2023). "Evidence and Importance of Intermediate Nanostructures in the Journey from Molecular Precursors to Allophane and Imogolite Nanocrystals". *Applied Clay Science*, 241. DOI: 10.1016/j.clay.2023.107013
- Pierzynski, G. M., McDowell, R. W., and Thomas Sims, J. (2005). "Chemistry, Cycling, and Potential Movement of Inorganic Phosphorus in Soils". In: *Phosphorus: Agriculture and the Environment*. John Wiley & Sons, Ltd. Chap. 3, pp. 51–86. doi: 10.2134/agronmonogr46.c3.
- Plassard, C., Louche, J., Ali, M. A., Duchemin, M., Legname, E., and Cloutier-Hurteau, B. (2011). "Diversity in Phosphorus Mobilisation and Uptake in Ectomycorrhizal Fungi". *Annals of Forest Science*, 68(1). DOI: 10.1007/s13595-010-0005-7
- Rosling, A. (2009). "Trees, Mycorrhiza and Minerals –Field Relevance of in Vitro Experiments". *Geomicrobiology Journal*, 26(6). DOI: 10.1080/01490450902929324
- Sassi, M., Chaka, A. M., and Rosso, K. M. (2021). "Ab Initio Thermodynamics Reveals the Nanocomposite Structure of Ferrihydrite". *Communications Chemistry*, 4(1). DOI: 10.1038/s42004-021-00562-7
- Schreider, K., Hofmann, D., Boy, J., Andrino, A., Fernandes Figueiredo, A., Sauheitl, L., and Guggenberger, G. (2022). "Mycorrhizal Mediated Partitioning of Phosphorus: Ectomycorrhizal (Populus x Canescens x Paxillus Involutus) Potential to Exploit Simultaneously Organic and Mineral Phosphorus Sources". *Frontiers in Soil Science*, 2. DOI: 10.3389/fsoil.2022.865517
- Shah, F., Schwenk, D., Nicolás, C., Persson, P., Hoffmeister, D., and Tunlid, A. (2015). "Involutin Is an Fe3+ Reductant Secreted by the Ectomycorrhizal Fungus Paxillus Involutus during Fenton-Based Decomposition of Organic Matter". *Applied and Environmental Microbiology*, 81(24). DOI: 10.1128/AEM.02312-15
- Sherman, D. M. and Randall, S. R. (2003). "Surface Complexation of Arsenic(V) to Iron(III) (Hydr)Oxides: Structural Mechanism from Ab Initio Molecular Geometries and EXAFS Spectroscopy". *Geochimica et Cosmochimica Acta*, 67(22). DOI: 10.1016/S0016-7037(03) 00237-0
- Sokolova, T. A. (2020). "Low-Molecular-Weight Organic Acids in Soils: Sources, Composition, Concentrations, and Functions: A Review". *Eurasian Soil Science*, 53(5). DOI: 10.1134/S1064229320050154
- Tiberg, C. (2016). "Metal Sorption to Ferrihydrite". Doctoral Thesis. Uppsala: Swedish University of Agricultural Sciences.
- Tiberg, C., Sjöstedt, C., Persson, I., and Gustafsson, J. P. (2013). "Phosphate Effects on Copper(II) and Lead(II) Sorption to Ferrihydrite". *Geochimica et Cosmochimica Acta*, 120. DOI: 10.1016/j.gca.2013.06.012

- Tuyishime, J. P. M., Adediran, G. A., Olsson, B. A., Spohn, M., Hillier, S., Klysubun, W., and Gustafsson, J. P. (2022). "Phosphorus Abundance and Speciation in Acid Forest Podzols Effect of Postglacial Weathering". *Geoderma*, 406. DOI: 10.1016/j.geoderma.2021.115500
- Tuyishime, J. P. M., Florén, T., Rivard, C., and Gustafsson, J. P. (2024). "Microscale Heterogeneity of Phosphorus Species Associated with Secondary Mineral Phases in the B Horizons of Two Boreal Podzols". *Chemical Geology*, 655. DOI: 10.1016/j.chemgeo.2024.122083
- Tuyishime, M. (2022). "Phosphorus Chemistry in Managed Forest Soils: Effects of Weathering and Wood Ash Fertilisation". Doctoral Thesis. Uppsala: Swedish University of Agricultural Sciences.
- Uchida, S., Hashimoto, Y., Takamoto, A., Noguchi, K., Klysubun, W., and Wang, S.-L. (2022). "Phosphate Binding to Allophane and Ferrihydrite with Implications for Volcanic Ash Soils". *Soil Science Society of America Journal*, 86(6). DOI: 10.1002/saj2.20463
- van Riemsdijk, W. H. and Hiemstra, T. (2006). "Chapter 8 The CD-MUSIC Model as a Framework for Interpreting Ion Adsorption on Metal (Hydr) Oxide Surfaces". In: *Interface Science and Technology*. Ed. by Lützenkirchen, J. Vol. 11. Surface Complexation Modelling. Elsevier, pp. 251–268. DOI: 10.1016/S1573-4285(06)80052-9.
- Vermeer, A. W. P., van Riemsdijk, W. H., and Koopal, L. K. (1998). "Adsorption of Humic Acid to Mineral Particles. 1. Specific and Electrostatic Interactions". *Langmuir*, 14(10). DOI: 10.1021/la970624r
- Wada, K. (1989). "Allophane and Imogolite. In 'Minerals in Soil Environments'. (Eds JB Dixon, SB Weed) Pp. 1051–1087". *Soil Science Society of America: Madison, WI*,
- Walker, T. W. and Syers, J. K. (1976). "The Fate of Phosphorus during Pedogenesis". *Geoderma*, 15(1). DOI: 10.1016/0016-7061(76)90066-5
- Wang, H., Zhu, J., Fu, Q.-L., Xiong, J.-W., Hong, C., Hu, H.-Q., and Violante, A. (2015). "Adsorption of Phosphate onto Ferrihydrite and Ferrihydrite-Humic Acid Complexes". *Pedosphere*, 25(3). DOI: 10.1016/S1002-0160(15)30008-4
- Wang, S., Du, P., Yuan, P., Liu, Y., Song, H., Zhou, J., Deng, L., and Liu, D. (2020). "Structural Alterations of Synthetic Allophane under Acidic Conditions: Implications for Understanding the Acidification of Allophanic Andosols". *Geoderma*, 376. DOI: 10.1016/j.geoderma. 2020.114561
- Yucelen, G. I., Choudhury, R. P., Leisen, J., Nair, S., and Beckham, H. W. (2012). "Defect Structures in Aluminosilicate Single-Walled Nanotubes: A Solid-State Nuclear Magnetic Resonance Investigation". *The Journal of Physical Chemistry C*, 116(32). DOI: 10.1021/jp3059728
- Zhu, C. and Anderson, G. (2002). Environmental Applications of Geochemical Modeling. 1st ed. Cambridge University Press. DOI: 10.1017/CB09780511606274.

## **Appendix**

## Recipe - Ferrihydrite Sythesis and Batch Experiment

(written by Jon-Petter Gustafsson, adapted by Lisa Deiglmayr)

#### Day 1

#### 1. Start Fh synthesis

- a. Add  $36 \text{ mM Fe}(NO_3)_3 \cdot 9 \text{ H}_2\text{O}$  and  $12 \text{ mM NaNO}_3$  in a 500 mL volumetric flask, add MilliQ water to the mark and mix.
- b. Transfer content to a minimum 550 mL polyethylene bottle with magnet.
- c. Prepare 4 M NaOH in 25 mL volumetric flask (4 g NaOH to 25 mL).
- d. Place the bottle with iron on a magnetic stirrer, remove the lid and start the stirring and check the pH with a pH electrode (make sure that the pH meter is properly calibrated). Add 4 M NaOH dropwise until pH = 8.0 (around 10 mL are needed).
- e. Remove the bottle from the stirrer, attach the lid, and let the bottle stand for approximately 16 hours (it is not a problem, if it is some hours more).

#### Day 2

#### 2. Finish Fh synthesis

- a. Prepare 0.1 M HNO<sub>3</sub>.
- b. Place the bottle with iron on the stirrer again and add the 0.1 M HNO<sub>3</sub> solution dropwise until pH reaches 4.6 (around 15 mL are needed).
- c. Leave the contents on the magnetic stirrer for at least 30 min to remove excess CO<sub>2</sub> and start all batch experiments directly after.

#### 3. Start Batch experiments

- a. Prepare all stock solutions needed according to the recipe. NaOH solution needs to be prepared freshly.
  - NaOH 4 mM
  - HNO<sub>3</sub> 4 mM
  - NaH<sub>2</sub>PO<sub>4</sub> 4 mM
  - C<sub>2</sub>Na<sub>2</sub>O<sub>4</sub> 4 mM
  - C<sub>6</sub>H<sub>11</sub>NaO<sub>7</sub> 4 mM
- b. Prepare all suspensions according to the recipe in the following order: First MilliQ water using a syringe and a scale, next Fh, next acid (HNO<sub>3</sub>) or base (NaOH), next any competing ion, in this case phosphate.
- c. Bring suspensions to the cold room (8 °C), let them adjust to the temperature and add the organic acid.
- d. Attach the lids on the bottles, place them in a rack and insert the racks in the over-end shaker.

e. Adjust the knob on the shaker to "4" and shake the samples for 24 hours.

#### Day 3

- 4. Phase separation and pH measurement
  - a. After the 24 hours equilibration time, stop the shaker and place the samples in the centrifuge. Centrifuge at 3000 rpm for a minimum of 20 minutes at 8 °C.
  - b. Calibrate the pH meter in the cold room (make sure the pH meter was standing in the cold room already overnight to adjust to the temperature).
  - c. Remove the bottles carefully from the centrifuge.
  - d. Use a plastic syringe to remove around 20 mL from the supernatant
  - e. and then attach an Acrodisc PF single-use filter to the syringe. Press sample through the filter into the scintillation bottle marked with the appropriate sample number, but let the first 1 mL go to waste.
  - f. Measure the pH on the unfiltered sample without stirring up the solid from the bottom. Alternatively, use a Biohit pipette and remove 5 mL of the supernatant and measure the pH in another scintillation bottle.
  - g. Put all samples in the freezer until analysis.

## **Recipe - Proto-Imogolite Synthesis**

(written by Tove Florén, adapted by Lisa Deiglmayr)

#### **Stock solutions**

**S1Al** = AlCl<sub>3</sub> salt diluted to 280 mmolL<sup>-1</sup> **S1Si**= Sodium silicate solution diluted to 280 mmolL<sup>-1</sup> **S1OH** = NaOH pellets diluted to 280 mmolL<sup>-1</sup>

#### Day 1

1. Fill up a small water bath with de-ionized water (not MilliQ water). Place it in a fume hood and set to  $95\,^{\circ}\text{C}$ .

#### 2. Prepare reagents

- a. **S1Al:** Weigh exactly 6.76 g AlCl<sub>3</sub>. Add to a 100 mL volumetric flask, add MilliQ water to the mark and mix.
- b. **S1Si** Add exactly 4.4 mL sodium silicate solution to a 100 mL volumetric flask using a pipette, add MilliQ water to the mark and mix.
- c. **S10H** Weigh exactly 2.24 g NaOH. Add to a 200 mL volumetric flask, add MilliQ water to the mark and mix.

#### 3. Set up workspace in the fume hood

- a. Place a 500 mL beaker with a magnet on a magnetic stirrer. Have a pH meter close by.
- b. Calibrate the pH meter.
- c. Set up a peristaltic pump with silicone tubing. Rinse with MilliQ water and empty.

#### 4. Synthesise PIM

- a. First add 80 mL S1Al to the 500 mL beaker, set the stirrer to 200 rpm and start (It is important that S1Al is added first, otherwise amorphous silicate is formed) Then add 40 mL S1Si. The pH should now be around 3.3. Al:Si ratio = 2:1.
- b. Add 160 mL S1OH to a 250 mL beaker. Place one end of the peristaltic pump tubing in the 200 mL beaker with S1OH solution and the other end in the 500 mL on the stirring plate. Make sure that the tube is deep into the Al-Si solution. Set the pump to 80% and start. NaOH will now be added to the Al-Si solution at a rate of 1 mL/min. The pH will slowly rise and there will be white gel-like flocs forming.
- c. After 1-1.5 hours, check that the pumping is proceeding as expected.
- d. Turn off the pump and remove the tubing when all of the 160 mL S1OH solution has been added. The pH should be around 4.2. Al:Si:OH ratio = 1:0.5:2
- e. Set the solution to rapid stirring (approx. 400 rpm depending on size of beaker and magnet) at ambient temperature for 1 hour.
- f. Transfer the reaction mixture to anaerobic glass bottles and seal them with rubber stoppers and crimp seals. Note! Do not fill the bottles to more than ¾ and do not push too hard with the crimp sealer. The seals should remain intact and not have any dents in them.

- g. Place the bottles in the hot water bath set to 95 °C. Make sure that the reaction mixture is below the water bath water level.
- h. Leave the reaction mixture in the water bath for 48 hours. Check on the water bath every day and fill up with water if needed. During this time the reaction mixture, containing nuclei, will polymerize into PIM.

#### Day 3

#### 5. Finish PIM synthesis

- a. Remove the reaction mixture from the water bath after 48 hours, turn the water bath off, and let the reaction mixture cool to room temperature. Transfer the solution to a beaker and measure the pH (around 3.6).
- b. Prepare a 1 molL<sup>-1</sup> NaOH solution and slowly add it with a pipette, under continuous stirring, until the pH is around 4.8 (When the pH is around 4.2/4.3, add the NaOH very slowly, if the pH goes above 5, a gel forms). In total around 6 mL to 10 mL are needed.

#### 6. Dialyze the PIM solution to remove leftover salts

- a. Cut 1 dm to 2 dm long sections of dialysis tubing and let them soak for 2 hours in MilliQ water. Take a new beaker or container large enough to fit the dialysis tubes and fill up with new MilliQ water. Create a fold at the bottom of each dialysis tube and clamp tight. Make sure there are no leaks.
- b. Fill up each tube with the PIM solution, fold and clamp the other end as well. Check for leaks.
- c. Place in MilliQ water and leave to dialyze for around 48 hours. Change the MilliQ water once during this time.
- d. Remove the tubes after 48 hours and transfer to polyethylene bottles. The suspension now contains  $80 \,\mathrm{mmol} L^{-1}$  Al. Store in the fridge for up to one month.

## Recipe - Batch Experiment Proto-Imogolite

(written by Tove Florén, adapted by Lisa Deiglmayr)

#### Day 1

- a. Prepare all stock solutions needed according to the recipe. NaOH solution needs to be prepared freshly.
  - NaNO<sub>3</sub> 40 mM
  - NaOH 4 mM
  - HNO<sub>3</sub> 4 mM
  - NaH<sub>2</sub>PO<sub>4</sub> 4 mM
  - C<sub>2</sub>Na<sub>2</sub>O<sub>4</sub> 4 mM
  - C<sub>6</sub>H<sub>11</sub>NaO<sub>7</sub> 4 mM

- b. Prepare all suspensions according to the recipe in the following order: First MilliQ water using a syringe and a scale, next NaNO<sub>3</sub>, next acid (HNO<sub>3</sub>) or base (NaOH), next any competing ion, in this case phosphate.
- c. Bring suspensions to the cold room (8 °C), let them adjust to the temperature and add first PIM, then the organic acid.
- d. Attach the lids on the bottles, place them in a rack and insert the racks in the end-over-end shaker. A maximum of 44 samples can be run in one shaker.
- e. Adjust the knob on the shaker to "4" and shake the samples for 24 hours.

#### Day 2

- a. Turn off the shaker after 24 hours and remove the samples.
- b. Calibrate the pH meter in the cold room (make sure the pH meter was standing in the cold room already overnight to adjust to the temperature).
- c. Measure the pH on uncentrifuged samples.
- d. Take out 10K MWCO Centrifugal Devices (Pall Corporation, Ann Arbor, MI, USA). First the filters have to be rinsed with diluted HNO<sub>3</sub> three times. Fill them up with diluted HNO<sub>3</sub> (in the top container), attach the lids and run them in the centrifuge for 10 minutes at 3500 rpm at 8 °C. Rinse them once with MilliQ water.
- e. Discard the rinsing water. Transfer around 20 mL of sample into each centrifugal device, start with the first set of replicates and centrifuge for 15 minutes at 3500 rpm at 8 °C.
- f. Rinse the centrifugal devices with MilliQ water again.
- g. Repeat this procedure with the other replicate in the same tube.
- h. Put all samples in the freezer until analysis.

**Table 4:** Series: Ferrihydrite + Phosphorus (Day 19). Amount of stock solutions added in pH dependent batch experiments with measured pH, DOC and Fe and P content from ICP-OES. Empty cells indicate that no addition of the respective component was made or that no measurement was taken for the results. DOC or P cells with a value of 0 indicate that no OC or P was added in this series, although this was not explicitly measured to confirm this.

Series	Sample name	H <sub>2</sub> O (mL)	36 mM Fh (mL)	4 mM HNO <sub>3</sub> (mL)	4 mM NaOH (mL)	4 mM PO <sub>4</sub> (mL)	4 mM GL/Ox (mL)	Sum (mL)	рН	DOC (mg/L)	Fe (mg/L)	P (mg/L)
	1.1 1.2	25.09 25.09	3.41 3.41	7.5 7.5		4 4		40 40	3.23 3.21	0 0	0.025 0.023	0.383 0.366
	2.1 2.2	27.59 27.59	3.41 3.41	5 5		4 4		40 40	3.46 3.48	0	0.004 0.003	0.577 0.588
	3.1 3.2	30.09 30.09	3.41 3.41	2.5 2.5		4 4		40 40	4.03 4.03	0	-0.005 -0.005	1.225 1.271
Day 19)	90.1	30.59 30.59	3.41 3.41	2 2		4 4		40 40	4.15 4.12	0	-0.006 -0.005	0.068 0.045
3 mM TOTFe with 0.4 mM P (Day 19)	91.1 91.2	31.09 31.09	3.41 3.41	1.5 1.5		4 4		40 40	4.51 4.48	0	-0.007 -0.006	0.112 0.096
ith 0.4 ı	4.1 4.2	31.59 31.59	3.41 3.41	1 1		4 4		40 40	5.24 5.23	0	-0.006 -0.005	2.822 2.819
OTFe w	5.1 5.2	32.09 32.09	3.41 3.41	0.5 0.5		4 4		40 40	5.75 5.78	0	0.006 0.004	3.569 3.340
mM To	6.1	32.59 32.59	3.41 3.41			4 4		40 40	6.15	0	0.034 0.058	4.492 3.966
Ψ,	7.1 7.2	32.09 32.09	3.41 3.41		0.5 0.5	4 4		40 40	6.44 6.45	0	0.037 0.094	5.534 4.186
	8.1	31.59 31.59	3.41 3.41		1 1	4 4		40 40	6.71 6.71	0	0.209 0.171	4.861 5.046
	9.1 9.2	31.09 31.09	3.41 3.41		1.5 1.5	4 4		40 40	6.95 6.94	0	0.026 0.291	5.246 5.365
	10.1 10.2	30.59 30.59	3.41 3.41		2 2	4 4		40 40	7.15 7.13	0	0.025 0.324	6.600 5.599
	10.11	30.09 30.09	3.41 3.41		2.5 2.5	4 4		40 40	7.47 7.45	0	0.040 0.338	4.149 4.197
	10.31 10.32	29.09 29.09	3.41 3.41		3.5 3.5	4 4		40 40	7.8 7.86	0	0.194 0.395	6.209 5.918

**Table 5:** Series: Ferrihydrite + Phosphorus (Day 0). Amount of stock solutions added in pH dependent batch experiments with measured pH, DOC and Fe and P content from ICP-OES. Empty cells indicate that no addition of the respective component was made or that no measurement was taken for the results. DOC or P cells with a value of 0 indicate that no OC or P was added in this series, although this was not explicitly measured to confirm this.

Series	Sample name	H <sub>2</sub> O (mL)	36 mM Fh (mL)	4 mM HNO <sub>3</sub> (mL)	4 mM NaOH (mL)	4 mM PO <sub>4</sub> (mL)	4 mM GL/Ox (mL)	Sum (mL)	pН	DOC (mg/L)	Fe (mg/L)	P (mg/L)
	1.3	25.09	3.41	7.5		4		40	3.24	0	0.266	0.006
	1.4	25.09	3.41	7.5		4		40	3.24	0	0.275	0.007
	2.3	27.59	3.41	5		4		40	3.47	0	0.084	0.011
	2.4	27.59	3.41	5		4		40	3.46	0	0.085	0.009
	3.3	30.09	3.41	2.5		4		40	3.9	0	0.004	0.022
	3.4	30.09	3.41	2.5		4		40	3.91	0	0.003	0.021
y 0)	90.3	30.59	3.41	2		4		40	4.14	0	0.000	0.036
(Da	90.4	30.59	3.41	2		4		40	4.15	0	0.000	0.033
1 P	91.3	31.09	3.41	1.5		4		40	4.46	0	0.000	0.064
m.	91.4	31.09	3.41	1.5		4		40	4.46	0	0.000	0.059
4.0	4.3	31.59	3.41	1		4		40	5.28	0	0.000	0.204
vith	4.4	31.59	3.41	1		4		40	5.28	0	0.024	0.240
3 mM TOTFe with 0.4 mM P (Day 0)	5.3	32.09	3.41	0.5		4		40	6.18	0	0.000	0.737
707	5.4	32.09	3.41	0.5		4		40	6.13	0	0.000	0.829
N	6.3	32.59	3.41			4		40	6.33	0	0.006	1.292
3 m	6.4	32.59	3.41			4		40	6.37	0	0.010	1.427
	7.3	32.09	3.41		0.5	4		40	6.73	0	0.006	1.925
	7.4	32.09	3.41		0.5	4		40	6.79	0	0.039	2.034
	8.3	31.59	3.41		1	4		40	6.95	0	0.008	2.316
	8.4	31.59	3.41		1	4		40	6.99	0	0.058	2.206
	9.3	31.09	3.41		1.5	4		40	7.17	0	0.008	2.564
	9.4	31.09	3.41		1.5	4		40	7.21	0	0.087	2.623
	10.3	30.59	3.41		2	4		40	7.4	0	0.013	3.077
	10.4	30.59	3.41		2	4		40	7.42	0	0.077	3.241
	10.13	30.09	3.41		2.5	4		40	7.52	0	0.010	3.740
	10.14	30.09	3.41		2.5	4		40	7.55	0	0.107	3.941
	10.33	29.09	3.41		3.5	4		40	7.96	0	0.009	4.770
	10.34	29.09	3.41		3.5	4		40	7.97	0	0.240	5.025

**Table 6:** Series: Ferrihydrite + *D*-Gluconate. Amount of stock solutions added in pH dependent batch experiments with measured pH, DOC and Fe and P content from ICP-OES. Empty cells indicate that no addition of the respective component was made or that no measurement was taken for the results. DOC or P cells with a value of 0 indicate that no OC or P was added in this series, although this was not explicitly measured to confirm this.

Series	Sample name	H <sub>2</sub> O (mL)	36 mM Fh (mL)	4 mM HNO <sub>3</sub> (mL)	4 mM NaOH (mL)	4 mM PO <sub>4</sub> (mL)	4 mM GL/Ox (mL)	Sum (mL)	pН	DOC (mg/L)	Fe (mg/L)	P (mg/L)
	11.1	25.09	3.41	7.5			4	40	3.23	6.122		0
	11.2	25.09	3.41	7.5			4	40	3.2	5.712		0
	12.3	30.09	3.41	2.5			4	40	3.9	8.382		0
	12.4	30.09	3.41	2.5			4	40	3.9	8.556		0
	13.1	31.59	3.41	1			4	40	4.22	5.210		0
	13.2	31.59	3.41	1			4	40	4.27	6.481		0
	14.3	32.09	3.41	0.5			4	40	4.7	9.773		0
3 mM TOTFe with 0.4 mM GL	14.4	32.09	3.41	0.5			4	40	4.68	9.744		0
mM	15.1	32.59	3.41				4	40	4.99	7.813	0.014	0
4.0	15.2	32.59	3.41				4	40	4.95	6.461	0.015	0
ith	16.3	32.09	3.41		0.5		4	40	5.85	12.216		0
ė,	16.4	32.09	3.41		0.5		4	40	5.85	12.152		0
07.	17.1	31.84	3.41		0.75		4	40	5.69	8.920	0.007	0
1 T	17.2	31.84	3.41		0.75		4	40	5.69	9.160	0.002	0
<i>m</i>	x17.1	31.74	3.41		0.85		4	40	6.12	13.392		0
(4)	x17.2	31.74	3.41		0.85		4	40	6.25	14.155		0
	18.3	31.59	3.41		1		4	40	6.37	14.389		0
	18.4	31.59	3.41		1		4	40	6.45	15.801		0
	19.3	31.09	3.41		1.5		4	40	6.87	16.262		0
	19.4	31.09	3.41		1.5		4	40	6.84	16.632		0
	20.3	30.59	3.41		2		4	40	7.09	18.471		0
	20.4	30.59	3.41		2		4	40	7.14	18.236		0
	x20.1	30.34	3.41		2.25		4	40	7.2	18.584		0
	x20.2	30.34	3.41		2.25		4	40	7.27	20.038		0
	23.1	29.09	3.41		3.5		4	40	8.12	18.581		0
	23.2	29.09	3.41		3.5		4	40	8.15	18.594		0
	24.1	28.59	3.41		4		4	40	9.35	20.448		0
	24.2	28.59	3.41		4		4	40	9.13	19.807		0

**Table 7:** Series: Ferrihydrite + Phosphorus + *D*-Gluconate. Amount of stock solutions added in pH dependent batch experiments with measured pH, DOC and Fe and P content from ICP-OES. Empty cells indicate that no addition of the respective component was made or that no measurement was taken for the results. DOC or P cells with a value of 0 indicate that no OC or P was added in this series, although this was not explicitly measured to confirm this.

Series	Sample name	H <sub>2</sub> O (mL)	36 mM Fh (mL)	4 mM HNO <sub>3</sub> (mL)	4 mM NaOH (mL)	4 mM PO <sub>4</sub> (mL)	4 mM GL/Ox (mL)	Sum (mL)	pН	DOC (mg/L)	Fe (mg/L)	P (mg/L)
	25.3	21.09	3.41	7.5		4	4	40	3.55	16.038	0.409	0.126
	25.4	21.09	3.41	7.5		4	4	40	3.5	13.325	0.476	0.172
	26.3	23.59	3.41	5		4	4	40	4.18	16.232	0.076	0.421
7:	26.4	23.59	3.41	5		4	4	40	3.84	20.469	0.134	0.272
M	27.3	26.09	3.41	2.5		4	4	40	4.66	21.050	0.018	0.540
4 m.	27.4	26.09	3.41	2.5		4	4	40	4.6	21.741	0.015	0.735
d 0.	28.3	26.59	3.41	2		4	4	40	5	22.303	0.008	0.844
3 mM TOTFe with 0.4 mM P and 0.4 mM GL	28.4	26.59	3.41	2		4	4	40	4.95	22.451	0.006	1.019
M	29.3	27.29	3.41	1.3		4	4	40	5.6	22.318	0.002	1.242
4 m	29.4	27.29	3.41	1.3		4	4	40	5.48	23.822	0.007	1.530
h 0.	30.3	27.59	3.41	1		4	4	40	5.87	24.874	0.061	1.801
wit	30.4	27.59	3.41	1		4	4	40	6.14	25.954	0.150	2.518
TFe	31.3	28.59	3.41			4	4	40	6.45	25.512	0.163	2.582
T0	31.4	28.59	3.41			4	4	40	6.33	25.538	0.174	2.926
nM	32.3	28.09	3.41		0.5	4	4	40	6.65	26.100	0.226	2.996
3,1	32.4	28.09	3.41		0.5	4	4	40	6.57	25.877	0.335	3.307
	33.3	27.59	3.41		1	4	4	40	6.86	26.012	0.306	3.361
	33.4	27.59	3.41		1	4	4	40	6.74	26.045	0.390	3.592
	34.3	27.09	3.41		1.5	4	4	40	7.08	26.209	0.487	3.793
	34.4	27.09	3.41		1.5	4	4	40	6.88	26.230	0.609	3.907
	35.3	26.59	3.41		2	4	4	40	7.25	26.581	0.424	4.088
	35.4	26.59	3.41		2	4	4	40	7.02	26.076	0.712	4.130
	36.3	26.09	3.41		2.5	4	4	40	7.36	26.255	0.438	4.746
	36.4	26.09	3.41		2.5	4	4	40	7.17	26.813	0.897	4.557

Series	Sample name	H <sub>2</sub> O (mL)	36 mM Fh (mL)	4 mM HNO <sub>3</sub> (mL)	4 mM NaOH (mL)	4 mM PO <sub>4</sub> (mL)	4 mM GL/Ox (mL)	Sum (mL)	pН	DOC (mg/L)	Fe (mg/L)	P (mg/L)
	40.1 40.2	25.09 25.09	3.41 3.41	7.5 7.5			4 4	40 40	3.71 3.72	1.990 1.864	3.269 2.894	0
	92.1 92.2	26.59 26.59	3.41 3.41	6 6			4 4	40 40	3.99 3.97	1.908 1.556		0
	93.1 93.2	27.59 27.59	3.41 3.41	5 5			4 4	40 40	4.45 4.48	1.557 1.268		0
	94.1 94.2	28.59 28.59	3.41 3.41	4 4			4 4	40 40	5.24 5.22	0.893 1.784		0
и ох	41.1 41.2	30.09 30.09	3.41 3.41	2.5 2.5			4 4	40 40	5.96 6.01	3.723 3.411	0.367 0.329	0
0.4 m]	42.1 42.2	31.59 31.59	3.41 3.41	1 1			4 4	40 40	6.46 6.48	4.935 5.106	0.010 0.010	0
3 mM TOTFe with 0.4 mM Ox	43.1 43.2	32.09 32.09	3.41 3.41	0.5 0.5			4 4	40 40	6.6 6.55	5.684 5.630	0.005 0.003	0
TOTF	44.1 44.2	32.59 32.59	3.41 3.41				4 4	40 40	6.68 6.69	6.282 6.520	0.001 0.000	0
3 mM	45.1 45.2	32.09 32.09	3.41 3.41		0.5 0.5		4 4	40 40	6.75 6.74	6.723 6.746	0.000	0
	46.1 46.2	31.84 31.84	3.41 3.41		0.75 0.75		4 4	40 40	6.69 6.69	6.887 6.904	0.000	0
	47.1 47.2	31.69 31.69	3.41 3.41		0.9 0.9		4 4	40 40	6.83 6.78	7.009 7.029	0.000	0
	48.1 48.2	31.59 31.59	3.41 3.41		1 1		4 4	40 40	6.75 6.76	7.383 7.227	0.000	0
	49.1 49.2	31.09 31.09	3.41 3.41		1.5 1.5		4 4	40 40	6.82 6.93	7.783 7.821		0
	50.1 50.2	30.59 30.59	3.41 3.41		2 2		4 4	40 40	6.96 7.03	7.680 8.397		0
	51.1 51.2	30.09 30.09	3.41 3.41		2.5 2.5		4 4	40 40	7.11 7.12	8.298 8.896		0
	52.1 52.2	29.59 29.59	3.41 3.41		3 3		4 4	40 40	7.34 7.4	8.969 9.305		0
	53.1 53.2	29.09 29.09	3.41 3.41		3.5 3.5		4 4	40 40	8.12 8.43	9.132 9.407		0
	54.1 54.2	27.59 27.59	3.41 3.41		5 5		4 4	40 40	9.89 9.56	8.484 9.661		0

**Table 9:** Series: Ferrihydrite + Phosphours + Oxalate. Amount of stock solutions added in pH dependent batch experiments with measured pH, DOC and Fe and P content from ICP-OES. Empty cells indicate that no addition of the respective component was made or that no measurement was taken for the results. DOC or P cells with a value of 0 indicate that no OC or P was added in this series, although this was not explicitly measured to confirm this.

Series	Sample name	H <sub>2</sub> O (mL)	36 mM Fh (mL)	4 mM HNO <sub>3</sub> (mL)	4 mM NaOH (mL)	4 mM PO <sub>4</sub> (mL)	4 mM GL/Ox (mL)	Sum (mL)	pН	DOC (mg/L)	Fe (mg/L)	P (mg/L)
	95.1 95.2	19.59 19.59	3.41 3.41	9		4 4	4	40 40	3.93 3.93	4.389 4.117	5.119 5.218	0.247 0.258
							·					
	56.1 56.2	21.09 21.09	3.41 3.41	7.5 7.5		4 4	4 4	40 40	4.21 4.26	4.284 4.073	4.367 4.314	0.439 0.413
0x	57.1	23.59	3.41	5		4	4	40	5.14	4.557	3.352	1.183
3 mM TOTFe with 0.4 mM P and 0.4 mM Ox	57.2	23.59	3.41	5		4	4	40	5.18	5.321	3.405	1.096
7.4	58.1	26.09	3.41	2.5		4	4	40	5.82	6.628	0.917	1.536
) pu	58.2	26.09	3.41	2.5		4	4	40	5.85	6.664	1.216	1.555
P a	59.1	26.59	3.41	2		4	4	40	5.97	7.000	0.577	1.674
mM	59.2	26.59	3.41	2		4	4	40	5.98	6.869	0.880	1.712
0.4	60.1	27.29	3.41	1.3		4	4	40	6.16	7.444	0.231	1.811
ith	60.2	27.29	3.41	1.3		4	4	40	6.15	7.303	0.535	1.825
e *	61.1	27.59	3.41	1		4	4	40	6.29	7.635	0.146	1.864
ОТ	61.2	27.59	3.41	1		4	4	40	6.3	8.152	0.370	1.917
NT	62.1	28.59	3.41			4	4	40	6.64	8.339	0.052	2.425
3 m	62.2	28.59	3.41			4	4	40	6.6	8.194	0.307	2.455
··•	63.1	28.09	3.41		0.5	4	4	40	6.76	8.461	0.025	2.581
	63.2	28.09	3.41		0.5	4	4	40	6.79	7.836	0.477	2.879
	65.1	27.09	3.41		1.5	4	4	40	7.06	8.810	0.031	3.208
	65.2	27.09	3.41		1.5	4	4	40	7.09	8.692	0.430	3.364
	66.1	26.09	3.41		2.5	4	4	40	7.41	8.941	0.051	4.071
	66.2	26.09	3.41		2.5	4	4	40	7.46	8.698	0.423	4.019
	67.1	25.09	3.41		3.5	4	4	40	7.72	8.679	0.074	5.136
	67.2	25.09	3.41		3.5	4	4	40	7.84	8.688	0.410	5.042
	68.1	23.59	3.41		5	4	4	40	8.24	9.241	0.154	6.494
	68.2	23.59	3.41		5	4	4	40	8.38	9.077	0.474	6.565

**Table 10:** Series: Proto-Imogolite + Phosphorus. Amount of stock solutions added in pH dependent batch experiments with measured pH, DOC and Al, Si and P content from ICP-OES. Empty cells indicate that no addition of the respective component was made or that no measurement was taken for the results. DOC or P cells with a value of 0 indicate that no OC or P was added in this series, although this was not explicitly measured to confirm this.

Series	Sample name	H <sub>2</sub> O (mL)	40 mM NaNO <sub>3</sub> (mL)	80 mM PIM (mL)	4 mM HNO <sub>3</sub> (mL)	4 mM NaOH (mL)	4 mM PO <sub>4</sub> (mL)	4 mM GL/Ox (mL)	Sum (mL)	pН	DOC (mg/L)	Al (mg/L)	Si (mg/L)	P (mg/L)
	0.1 0.2	15.5 15.5	10 10	1.5 1.5	9 9		4 4		40 40	4.07 4.08	0	5.095 5.469	1.776 1.720	1.074 1.164
	2.1 2.2	18.5 18.5	10 10	1.5 1.5	6 6		4 4		40 40	4.29 4.25	0	3.437 2.367	1.173 0.941	0.418 0.305
	4.1 4.2	22.5 22.5	10 10	1.5 1.5	2 2		4 4		40 40	4.63 4.57	0	1.369 2.299	0.923 1.570	0.253 0.412
Ь	6.1 6.2	23.5 23.5	10 10	1.5 1.5	1 1		4 4		40 40	4.89 4.89	0	0.099 0.086	0.526 0.611	0.145 0.167
3 mM TOTAl with 0.4 mM	7.1 7.2	24 24	10 10	1.5 1.5	0.5 0.5		4 4		40 40	5.17 5.23	0	0.022 0.006	0.473 0.221	0.201 0.214
I with 6	8.1 8.2	24.5 24.5	10 10	1.5 1.5			4 4		40 40	5.73 5.6	0	-0.001 0.018	0.113 0.107	0.321 0.187
4 тота	9.1 9.2	24 24	10 10	1.5 1.5		0.5 0.5	4 4		40 40	5.95 6	0	0.005 0.001	0.123 0.124	0.358 0.492
3 тЛ	10.1 10.2	23.75 23.75	10 10	1.5 1.5		0.75 0.75	4 4		40 40	6.13 6.15	0	0.000 0.006	0.121 0.161	0.463 0.435
	11.1 11.2	23.5 23.5	10 10	1.5 1.5		1 1	4 4		40 40	6.28 6.37	0	0.001 0.001	0.119 0.127	0.535 0.556
	12.1	23 23	10 10	1.5 1.5		1.5 1.5	4 4		40 40	6.63	0	0.001 0.001	0.131 0.139	0.767 0.783
	13.1 13.2 13.3	22 22 22	10 10 10	1.5 1.5 1.5		2.5 2.5 2.5	4 4 4		40 40 40	7.2 7 7.24	0 0 0	0.002 -0.001 0.000	0.103 0.089 0.139	2.146 2.824 2.449
	14.1 14.2 14.3	21 21 21	10 10 10	1.5 1.5 1.5		3.5 3.5 3.5	4 4 4		40 40 40	7.65 7.37 7.65	0 0 0	0.001 0.000 0.004	0.086 0.058 0.147	2.238 1.983 3.603
	15.1 15.2 15.3	19.5 19.5 19.5	10 10 10	1.5 1.5 1.5		5 5 5	4 4 4		40 40 40	8.17 7.72 8.03	0 0 0	0.019 0.007 0.030	0.099 0.055 0.132	4.280 3.724 4.370

**Table 11:** Series: Proto-Imogolite + *D*-Gluconate. Amount of stock solutions added in pH dependent batch experiments with measured pH, DOC and Al, Si and P content from ICP-OES. Empty cells indicate that no addition of the respective component was made or that no measurement was taken for the results. DOC or P cells with a value of 0 indicate that no OC or P was added in this series, although this was not explicitly measured to confirm this.

Series	Sample name	H <sub>2</sub> O (mL)	40 mM NaNO <sub>3</sub> (mL)	80 mM PIM (mL)	4 mM HNO <sub>3</sub> (mL)	4 mM NaOH (mL)	4 mM PO <sub>4</sub> (mL)	4 mM GL/Ox (mL)	Sum (mL)	pН	DOC (mg/L)	Al (mg/L)	Si (mg/L)	P (mg/L)
	18.1 18.2	12.5 12.5	10 10	1.5 1.5	12 12			4 4	40 40	4.19 4.18	23.047 28.910	35.258		0
	19.1 19.2	15.5 15.5	10 10	1.5 1.5	9			4 4	40 40	4.36 4.38	18.967 25.564	10.297		0
	20.1 20.2	17.5 17.5	10 10	1.5 1.5	7 7			4 4	40 40	4.67 4.64	20.888 15.322	8.019		0
	20.3 20.4	17.5 17.5	10 10	1.5 1.5	7 7			4 4	40 40	4.54 4.57	14.412 19.210	8.208		0
	21.1 21.2	18.5 18.5	10 10	1.5 1.5	6 6			4 4	40 40	4.65 4.66	16.114 15.520	5.508		0
ıM GL	22.1 22.2	20.5 20.5	10 10	1.5 1.5	4 4			4 4	40 40	4.83 4.84	11.585 12.360	2.848		0
th 0.4 n	23.1 23.2	22.5 22.5	10 10	1.5 1.5	2 2			4 4	40 40	5.06 5.05	17.330 12.218	2.479		0
3 mM TOTAI with 0.4 mM GL	24.1 24.2	23 23	10 10	1.5 1.5	1.5 1.5			4 4	40 40	5.14 5.13	14.049 11.774	1.925		0
nM TO	25.1 25.2	23.5 23.5	10 10	1.5 1.5	1 1			4 4	40 40	5.25 5.28	13.546 12.151			0
3,1	26.1 26.2	24 24	10 10	1.5 1.5	0.5 0.5			4 4	40 40	5.44 5.38	16.177 11.252			0
	27.1	24.5 24.5	10 10	1.5 1.5				4 4	40 40	5.51 5.55	10.517 11.532			0
	28.1 28.2	24 24	10 10	1.5 1.5		0.5 0.5		4 4	40 40	5.73 6.06	15.610 19.051			0
	29.1 29.2	23.75 23.75	10 10	1.5 1.5		0.75 0.75		4 4	40 40	5.85 6.03	15.394 15.184			0
	30.1 30.2	23.5 23.5	10 10	1.5 1.5		1 1		4 4	40 40	6.03 6.04	12.674			0
	31.1 31.2	23 23	10 10	1.5 1.5		1.5 1.5		4 4	40 40	6.37 6.51	11.934 13.559			0
	32.1 32.2	23 23	10 10	1.5 1.5		1.5 1.5		4 4	40 40	6.52 6.64	11.510 22.519			0
	33.1 33.2	22 22	10 10	1.5 1.5		2.5 2.5		4 4	40 40	7.24 7.15	16.290 24.179			0
	34.1 34.2	21 21	10 10	1.5 1.5		3.5 3.5		4 4	40 40	7.96 7.6	16.903 25.621			0
	35.1 35.2	19.5 19.5	10 10	1.5 1.5		5 5		4 4	40 40	8.8 8.7	19.270 26.564			0

**Table 12:** Series: Proto-Imogolite + Phosphorus + *D*-Gluconate. Amount of stock solutions added in pH dependent batch experiments with measured pH, DOC and Al, Si and P content from ICP-OES. Empty cells indicate that no addition of the respective component was made or that no measurement was taken for the results. DOC or P cells with a value of 0 indicate that no OC or P was added in this series, although this was not explicitly measured to confirm this.

Series	Sample name	H <sub>2</sub> O (mL)	40 mM NaNO <sub>3</sub> (mL)	80 mM PIM (mL)	4 mM HNO <sub>3</sub> (mL)	4 mM NaOH (mL)	4 mM PO <sub>4</sub> (mL)	4 mM GL/Ox (mL)	Sum (mL)	pН	DOC (mg/L)	Al (mg/L)	Si (mg/L)	P (mg/L)
	38.1 38.2	7.5 7.5	10 10	1.5 1.5	13 13		4 4	4 4	40 40	3.9 3.89	18.110 24.629	11.579 12.007	4.165 4.032	2.655 2.893
	41.1 41.2	13.5 13.5	10 10	1.5 1.5	7 7		4 4	4 4	40 40	4.14 4.14	25.416 19.322	3.929 3.681	1.390 1.499	1.340 1.287
	42.1 42.2	16.5 16.5	10 10	1.5 1.5	4 4		4 4	4 4	40 40	4.42 4.44	26.981 18.803	1.529 1.622	0.903 1.109	0.977 1.003
nM GL	43.1	18.5 18.5	10 10	1.5 1.5	2 2		4 4	4	40 40	4.93 4.94	23.132 20.587	0.328 0.302	0.467 0.489	1.028 1.046
nd 0.4 1	44.1	19 19	10 10	1.5 1.5	1.5 1.5		4 4	4	40 40	5.18 5.22	21.690 22.036	0.255 0.171	0.389 0.407	1.167 1.243
3 mM TOTAI with 0.4mM P and 0.4 mM GL	45.1 45.2	19.5 19.5	10 10	1.5 1.5	1 1		4 4	4 4	40 40	5.53 5.5	18.361 22.264	0.079 0.077	0.256 0.314	0.698 1.561
vith 0.4	46.1 46.2	20 20	10 10	1.5 1.5	0.5 0.5		4 4	4 4	40 40	5.82 5.83	29.195 23.730	0.031 0.038	0.209 0.217	2.009 1.931
TOTAL	47.1 47.2	20.5 20.5	10 10	1.5 1.5			4 4	4 4	40 40	6.22 6.19	28.587 25.192	0.024 0.020	0.165 0.208	2.548 2.406
3 mM	48.1 48.2	20 20	10 10	1.5 1.5		0.5 0.5	4 4	4 4	40 40	6.43 6.49	27.648 26.450	0.007 0.011	0.144 0.130	2.628 2.850
	49.1 49.2	19.75 19.75	10 10	1.5 1.5		0.75 0.75	4	4 4	40 40	6.62 6.62	31.158 26.377	0.011 0.016	0.109 0.125	3.171 3.193
	51.1 51.2	19 19	10 10	1.5 1.5		1.5 1.5	4 4	4 4	40 40	6.83 6.87	29.262 27.034	0.001 0.012	0.098 0.116	3.652 4.047
	52.1 52.2	18 18	10 10	1.5 1.5		2.5 2.5	4 4	4 4	40 40	7.25 7.21	24.006 26.244	0.000 0.002	0.084 0.093	2.950 3.551
	53.1 53.2	17 17	10 10	1.5 1.5		3.5 3.5	4 4	4 4	40 40	7.68 7.62	30.323 25.799	0.018 0.031	0.119 0.102	4.422 4.307
	54.1 54.2	15.5 15.5	10 10	1.5 1.5		5 5	4 4	4 4	40 40	8.19 8.05	21.726 12.015	0.056 0.026	0.089 0.094	4.819 5.227
	55.1 55.2	14.5 14.5	10 10	1.5 1.5		6	4 4	4 4	40 40	8.34 8.15	26.942 36.500	0.064 0.074	0.108 0.105	5.832 5.782

**Table 13:** Series: Proto-Imogolite + Oxalate. Amount of stock solutions added in pH dependent batch experiments with measured pH, DOC and Al, Si and P content from ICP-OES. Empty cells indicate that no addition of the respective component was made or that no measurement was taken for the results. DOC or P cells with a value of 0 indicate that no OC or P was added in this series, although this was not explicitly measured to confirm this.

Series	Sample name	H <sub>2</sub> O (mL)	40 mM NaNO <sub>3</sub> (mL)	80 mM PIM (mL)	4 mM HNO <sub>3</sub> (mL)	4 mM NaOH (mL)	4 mM PO <sub>4</sub> (mL)	4 mM GL/Ox (mL)	Sum (mL)	pН	DOC (mg/L)	Al (mg/L)	Si (mg/L)	P (mg/L)
	58.1 58.2	4.5 4.5	10 10	1.5 1.5	20 20			4 4	40 40	4.12 4.12	8.090 14.048	18.740		0 0
	59.1 59.2	9.5 9.5	10 10	1.5 1.5	15 15			4 4	40 40	4.34 4.38	7.266 17.273	12.121		0
	60.1 60.2	13.5 13.5	10 10	1.5 1.5	11 11			4 4	40 40	4.5 4.51	6.941 16.619	8.681		0
	61.1 61.2	15.5 15.5	10 10	1.5 1.5	9 9			4 4	40 40	4.68 4.65	6.766 16.068	10.167		0
o <sub>x</sub>	62.1	17.5 17.5	10 10	1.5 1.5	7 7			4 4	40 40	4.92 4.92	7.012 14.977	4.720		0
3 mM TOTAl with 0.4mM Ox	75.1 75.2	19 19	10 10	1.5 1.5	5.5 5.5			4 4	40 40	5.23 5.24	5.509 14.543	5.888		0
41 with	63.1	20.5 20.5	10 10	1.5 1.5	4 4			4 4	40 40	5.88 5.63	4.871 13.241	1.917		0
м тот	76.1 76.2	21.5 21.5	10 10	1.5 1.5	3 3			4 4	40 40	6.02 5.95	4.747 10.083	1.517		0
3 m	64.1 64.2	22.5 22.5	10 10	1.5 1.5	2 2			4 4	40 40	6.44 6.43	5.005 11.854	0.909		0
	65.1 65.2	23 23	10 10	1.5 1.5	1.5 1.5			4 4	40 40	6.61 5.57	5.070 11.479	0.640		0
	66.1	23.5 23.5	10 10	1.5 1.5	1 1			4 4	40 40	6.82 6.78	5.294 13.089	0.347		0
	67.1 67.2	24 24	10 10	1.5 1.5	0.5 0.5			4 4	40 40	6.93 6.96	5.589 11.688	0.182		0
	68.1 68.2	24.5 24.5	10 10	1.5 1.5				4 4	40 40	7.15 7.03	4.996 15.828	0.097		0
	69.1 69.2	24 24	10 10	1.5 1.5		0.5 0.5		4 4	40 40	7.54 7.48	5.920 12.622	0.085		0
	70.1 70.2	23.5 23.5	10 10	1.5 1.5		1 1		4 4	40 40	7.86 7.93	7.273 16.060			0
	71.1 71.2	23 23	10 10	1.5 1.5		1.5 1.5		4 4	40 40	8.01 8.07	6.205 12.911			0
-	72.1 72.2	22 22	10 10	1.5 1.5		2.5 2.5		4 4	40 40	8.34 8.47	7.238 13.929			0

**Table 14:** Series: Proto-Imogolite + Phosphorus + Oxalate. Amount of stock solutions added in pH dependent batch experiments with measured pH, DOC and Al, Si and P content from ICP-OES. Empty cells indicate that no addition of the respective component was made or that no measurement was taken for the results. DOC or P cells with a value of 0 indicate that no OC or P was added in this series, although this was not explicitly measured to confirm this.

Series	Sample name	H <sub>2</sub> O (mL)	40 mM NaNO <sub>3</sub> (mL)	80 mM PIM (mL)	4 mM HNO <sub>3</sub> (mL)	4 mM NaOH (mL)	4 mM PO <sub>4</sub> (mL)	4 mM GL/Ox (mL)	Sum (mL)	pН	DOC (mg/L)	Al (mg/L)	Si (mg/L)	P (mg/L)
	80.1 80.2	0.5 0.5	10 10	1.5 1.5	20 20		4 4	4 4	40 40	3.77 3.74	6.546 17.936	15.846 17.383	4.417 4.644	3.286 4.279
	82.1 82.2	9.5 9.5	10 10	1.5 1.5	11 11		4 4	4 4	40 40	4.23 4.24	7.093 16.717	7.088 7.450	2.145 2.126	2.086 2.249
M Ox	83.1 83.2	11.5 11.5	10 10	1.5 1.5	9 9		4 4	4 4	40 40	4.46 4.49	6.843 14.731	5.416 5.466	1.738 1.743	2.099 2.170
3 mM TOTAl with 0.4mM P and 0.4 mM Ox	84.1 84.2	13.5 13.5	10 10	1.5 1.5	7 7		4 4	4 4	40 40	4.88 4.89	8.347 17.237	3.764 3.776	1.370 1.332	2.293 2.329
ıM P an	85.1 85.2	14.5 14.5	10 10	1.5 1.5	6 6		4 4	4 4	40 40	5.19 5.25	6.931 17.471	3.128 3.172	1.237 1.221	2.625 2.612
ith 0.4m	86.1 86.2	15.5 15.5	10 10	1.5 1.5	5 5		4 4	4 4	40 40	5.56 5.55	6.492 15.082	2.605 2.521	1.021 0.950	2.971 2.958
OTAI w	87.1 87.2	16.5 16.5	10 10	1.5 1.5	4 4		4 4	4 4	40 40	5.87 5.86	7.207 15.713	2.093 2.113	0.594 0.564	3.267 3.335
8 mM T	88.1 88.2	17.5 17.5	10 10	1.5 1.5	3 3		4 4	4 4	40 40	6.11 6.12	7.161 17.310	1.572 1.562	0.328 0.328	3.504 3.524
ω,	90.1	19 19	10 10	1.5 1.5	1.5 1.5		4 4	4 4	40 40	6.44 6.43	8.973 14.542	0.849 0.782	0.278 0.236	3.579 3.527
	91.1 91.2	19.5 19.5	10 10	1.5 1.5	1 1		4 4	4 4	40 40	6.55 6.57	7.894 18.551	0.608 0.572	0.202 0.236	3.491 3.359
	94.1 94.2	20 20	10 10	1.5 1.5		0.5 0.5	4 4	4 4	40 40	6.92 6.89	9.605 18.065	0.181 0.170	0.137 0.183	3.620 3.683
	95.1 95.2	19 19	10 10	1.5 1.5		1.5 1.5	4 4	4 4	40 40	7.17 7.19	9.110 20.091	0.063 0.056	0.159 0.151	3.871 3.891
	96.1	18 18	10 10	1.5 1.5		2.5 2.5	4 4	4 4	40 40	7.49 7.46	10.297 17.960	0.027 0.016	0.119 0.127	4.113 4.144

# **Publishing and Archiving**

Approved students' theses at SLU can be published online. As a student you own the copyright to your work and in such cases, you need to approve the publication. In connection with your approval of publication, SLU will process your personal data (name) to make the work searchable on the internet. You can revoke your consent at any time by contacting the library.

Even if you choose not to publish the work or if you revoke your approval, the thesis will be archived digitally according to archive legislation. You will find links to SLU's publication agreement and SLU's processing of personal data and your rights on this page:

https://libanswers.slu.se/en/faq/228318

X	YES, I, Lisa Deiglmayr, have read and agree to the agreement for publication	and the
	personal data processing that takes place in connection with this.	

Ш	NO, I, Lisa Deiglmayr, do not give my permission to publish the full text of this work
	However, the work will be uploaded for archiving and the metadata and summary will be
	visible and searchable.